Monthly Notices
of the
ROYAL ASTRONOMICAL SOCIETY

MNRAS **506,** 1761–1776 (2021)
Advance Access publication 2021 June 21

https://doi.org/10.1093/mnras/stab1086

Fundamental relations for the velocity dispersion of stars in the Milky Way

Sanjib Sharma [1,2]★ Michael R. Hayden,[1,2] Joss Bland-Hawthorn [1,2] Dennis Stello,[2,3,4] Sven Buder [2,5,6] Joel C. Zinn,[3] Thomas Kallinger,[7] Martin Asplund,[8] Gayandhi M. De Silva,[9] Valentina D'Orazi,[10] Ken Freeman,[6] Janez Kos,[11] Geraint F. Lewis [1] Jane Lin,[6] Karin Lind,[12] Sarah Martell [2,3] Jeffrey D. Simpson [3] Rob A. Wittenmyer [13] Daniel B. Zucker,[9,14] Tomaz Zwitter [11] Boquan Chen,[1] Klemen Cotar [11] James Esdaile,[3] Marc Hon [3] Jonathan Horner [13] Daniel Huber,[15] Prajwal R. Kafle,[16] Shourya Khanna [1] Yuan-Sen Ting,[6,17,18,19] David M. Nataf [20] Thomas Nordlander [2,6] Mohd Hafiz Mohd Saadon,[3,21] Thor Tepper-Garcia,[22] C. G. Tinney,[23] Gregor Traven,[24] Fred Watson,[25] Duncan Wright[13] and Rosemary F. G. Wyse [20]

Affiliations are listed at the end of the paper

Accepted 2021 April 9. Received 2021 April 8; in original form 2020 April 14

ABSTRACT

We explore the fundamental relations governing the radial and vertical velocity dispersions of stars in the Milky Way, from combined studies of complementary surveys including GALAH, LAMOST, APOGEE, the NASA *Kepler* and K2 missions, and *Gaia* DR2. We find that different stellar samples, even though they target different tracer populations and employ a variety of age estimation techniques, follow the same set of fundamental relations. We provide the clearest evidence to date that, in addition to the well-known dependence on stellar age, the velocity dispersions of stars depend on orbital angular momentum L_z, metallicity, and height above the plane $|z|$, and are well described by a multiplicatively separable functional form. The dispersions have a power-law dependence on age with exponents of 0.441 ± 0.007 and 0.251 ± 0.006 for σ_z and σ_R, respectively, and the power law is valid even for the oldest stars. For the solar neighbourhood stars, the apparent break in the power law for older stars, as seen in previous studies, is due to the anticorrelation of L_z with age. The dispersions decrease with increasing L_z until we reach the Sun's orbital angular momentum, after which σ_z increases (implying flaring in the outer disc) while σ_R flattens. For a given age, the dispersions increase with decreasing metallicity, suggesting that the dispersions increase with birth radius. The dispersions also increase linearly with $|z|$. The same set of relations that work in the solar neighbourhood also work for stars between $3 < R/\mathrm{kpc} < 20$. Finally, the high-[α/Fe] stars follow the same relations as the low-[α/Fe] stars.

Key words: Galaxy: disc – Galaxy: evolution – Galaxy: formation – Galaxy: kinematics and dynamics.

1 INTRODUCTION

Most stars of the Milky Way's disc population are thought to be born on roughly circular orbits with very low velocity dispersion. However, a significant fraction of these stars are observed to have very high velocity dispersion, suggesting that they must have undergone significant dynamical evolution. Studying the velocity distributions for disc stars can therefore shed light not only on the dynamical history of the Galaxy but also on the dynamical processes that have shaped the present-day distribution of stars. Moreover, velocity dispersion relations are an essential ingredient for constructing analytical models of the Galaxy. Multiple studies have sought to characterize the velocity dispersion of stars in the Milky Way disc and to explain them using dynamical models. Despite much progress, however, many open questions remain.

1.1 Background

It has been known for a long time that the velocity dispersion of disc stars increases with age in the solar neighbourhood. One of the earliest attempts to explain this observation dates back to Spitzer & Schwarzschild (1951), who examined in-plane motions of disc stars. They showed that the total dispersion of all components, $\sigma_{\rm tot}$, increases with age τ due to scattering from massive clouds with a power-law dependence, $\tau^{\beta_{\rm tot}}$, with exponent $\beta_{\rm tot} = 0.33$. Remarkably, they inferred the presence of giant molecular clouds (GMCs) long before they were observed directly. Later, Lacey (1984) generalized this result by including vertical motions. However, the predictions of his model conflicted with observations. First, Lacey concluded that $\beta_{\rm tot} = 0.25$, whereas observations suggest that solar-neighbourhood stars have $\beta_{\rm tot}$ between 0.3 and 0.5 – or more precisely that β_z ranges from 0.35 to 0.6 and β_R ranges from 0.19 to 0.35 (Nordström et al. 2004; Aumer & Binney 2009; Sharma et al. 2014; Mackereth et al. 2019). Secondly, the overall heating rate derived (which determines the dispersion of older stars) was too low. Finally, Lacey predicted the ratio of vertical to radial dispersion, σ_z/σ_R, to be 0.8, which

★ E-mail: sanjib.sharma@gmail.com

© 2021 The Author(s)
Published by Oxford University Press on behalf of Royal Astronomical Society

Downloaded from https://academic.oup.com/mnras/article/506/2/1761/6307041 by INAF Trieste (Osservatorio Astronomico di Trieste) user on 13 April 2022

is higher than observed ratio for stars in the solar neighbourhood (0.5–0.6).

Hänninen & Flynn (2002) used *N*-body simulations to confirm some of the findings of Lacey (1984). They found that for scattering from GMCs, $\beta_{\rm tot}$ is indeed less than 0.33, or more precisely that $\beta_R = 0.20$, $\beta_z = 0.26$, and $\beta_{\rm tot} = 0.21$, which is even less than the value predicted by Lacey. The overall heating rate was also confirmed to be low. Specifically, with the surface density of GMCs set to the present-day value in the solar neighbourhood (5 $M_\odot$ pc^{-2}), the predicted velocity dispersion for the oldest stars was less than that of the observations by about 15 km s^{-1}. Additionally, Hänninen & Flynn (2002) found that the ratio σ_z/σ_R depends on the number density of GMCs. For the GMC number density of 5 $M_\odot$ pc^{-2}, σ_z/σ_R was 0.5 in rough agreement with the observed value, but much less than the value of Lacey (1984). The value of σ_z/σ_R computed by Lacey (1984) was large because an isotropic distribution of star-cloud impact parameters was assumed. When the anisotropy in the impact parameters is taken into account, σ_z/σ_R is 0.62 in the steady state (Ida, Kokubo & Makino 1993; Shiidsuka & Ida 1999; Sellwood 2008). This value of the ratio agrees well with the observations. For example, for 10-Gyr-old stars, Aumer & Binney (2009) report the ratio to be 0.56 using the Geneva Copenhagen survey (GCS; Nordström et al. 2004), while Sharma et al. (2014) report values of 0.59 and 0.65 using the GCS and RAVE surveys, respectively.

The inability of GMC scattering models to match the observed data prompted the exploration of other mechanisms to excite random motions. Transient spiral structures are one such mechanism. They lead to potential fluctuations in the disc that can heat up disc stars (Barbanis & Woltjer 1967; Sellwood & Carlberg 1984; Carlberg & Sellwood 1985). De Simone, Wu & Tremaine (2004) showed using numerical experiments in two dimensions that spiral arms alone can lead to β_R in the range 0.25–0.5, and a heating rate such that the value of σ_R is consistent with observations. However, spiral scattering is too inefficient to increase the vertical dispersion (Sellwood 2013; Martinez-Medina et al. 2015). This led Jenkins & Binney (1990) to argue that a combination of spiral structure and GMC heating could explain the velocity dispersion of observed stars, though their predicted β_z (0.3) was too low and the predicted β_R (0.5) was too large.

One way to resolve the discrepancy between the predicted and the observed values of β_z is to accommodate a scattering environment *that is evolving with time*. This consequently means that the velocity dispersion as a function of age (age–velocity relation or AVR) for stars in the solar neighbourhood is not same as the evolution of velocity dispersion with time of stars born together (heating history) at a given time in the past. In other words, the AVR is the compilation of the end of the heating history of stellar populations born at different times. Specifically, due to the much higher gas fraction in the early Galactic disc, the contribution of GMC scattering is expected to decrease with time, which has been shown to lead to β_z being close to 0.25 for the heating history but greater than 0.4 for the AVR (Aumer, Binney & Schönrich 2016a; Ting & Rix 2019).

There are other physical processes that can heat up the disc, and so shape the AVR. The Milky Way hosts a bar that can heat disc stars, as demonstrated in isolated disc/bar/bulge simulations (e.g. Saha, Tseng & Taam 2010), particularly near the strong Lindblad resonances. The same effect is seen in cosmological *N*-body simulations, where bars emerge within the evolving disc (Grand et al. 2016). But here there is an added contribution from the disc being bombarded by orbiting satellites (Velazquez & White 1999). Multiple disc asymmetric patterns moving at different pattern speed, such as multiple spirals (Minchev & Quillen 2006) or bar and spiral structure (Minchev & Famaey 2010) can also heat up the disc. The AVR can also be shaped by the fact that the intrinsic velocity dispersion was higher at earlier times, as reported by H α emission of gas in external galaxies at high redshift (Förster Schreiber et al. 2009; Wisnioski et al. 2015). However, H α emission tracks ionized gas and it is not yet clear, if stars, which form out of cold gas, also have high-velocity dispersion like the ionized gas. There is now strong evidence, both theoretical (Sellwood & Binney 2002; Roškar et al. 2008) and observational, that stars migrate from their place of birth. The observational evidence comes from the presence of low-eccentricity and super-metallicity stars in the solar neighbourhood – a realization that dates back to at least Grenon (1972; see also Kordopatis et al. 2015; Hayden et al. 2020). Because the heating rate is higher in the inner regions than in the outer regions, one has to take migration into account when modelling the AVR at a given location. However, in a comprehensive review of stellar migration, Minchev (2016) argues that migration, on average, generally does not lead to disc heating.

1.2 Modelling the physical mechanisms of disc evolution

Given that various physical processes can play a role in disc evolution, it is imperative to study them both individually (to assess their relative importance) and in combination (to see the full effect of them acting together). The seminal work by Aumer et al. (2016a) highlights the utility of this approach. They analysed N-body simulations that had spiral arms, GMCs, a bar, and growing discs – and were successful in reproducing the AVR in the solar neighbourhood of the Milky Way. However, this model was only compared with observations in the solar neighbourhood, and possible dependencies on metallicity and angular momentum were not considered. We show for the first time that these properties taken together can place even stronger constraints on the models.

There are also other good reasons for studying the dependence of velocity dispersion on metallicity and angular momentum. For a given age, the metallicity provides a way to tag the birth radius of a star, which provides leverage on the process of radial migration (Bland-Hawthorn, Krumholz & Freeman 2010; Frankel et al. 2019). The angular momentum L_z provides the mean radius where a star spends most of its history, and so (unlike the present radius R) is a more useful indicator of the amount of scattering the star has undergone. Moreover, there are strong theoretical reasons to prefer L_z over R. For an axisymmetric system L_z is a constant of motion and, Jeans' theorem tells us that the phase-space density of a system in dynamical equilibrium should only depend on constants of motion (Binney & Tremaine 2008). Furthermore, specifying the dispersion as a function of L_z paves the way for constructing better analytical models of the Galaxy, e.g. dynamical models based on actions by Binney (2012) and Sanders & Binney (2015).

Given that the velocity dispersion of a population of stars can depend on a number of stellar properties, it is important to come up with a useful way to characterize the velocity dispersion from observations such that it can test theoretical models. The selection function of a survey will tend to leave its imprint on the measured velocity dispersions (Sharma et al. 2014), which makes it difficult to compare and combine results from different surveys, and also to compare observed dispersions with model predictions. If the velocity dispersion σ only depends on a set of observables X, then knowing X is sufficient to characterize the dispersion irrespective of the selection function. This brings us to the question of identifying the fundamental relations governing the dispersion, i.e. what is a suitable choice for the set of observables/variables X, and how does the velocity dispersion depend on them. Intuitively (as discussed

Downloaded from https://academic.oup.com/mnras/article/506/2/1761/6307041 by INAF Trieste (Osservatorio Astronomico di Trieste) user on 13 April 2022

above) the dispersion should be governed by age, metallicity, and angular momentum. However, the joint dependence of dispersion on these properties has not been studied before, and this is what we address in this paper. Since stars migrate from their place of birth, strictly speaking, the amount of scattering a star experiences will also depend upon the evolutionary history of its angular momentum L_z, but we do not consider this as we do not have any observable that tracks this information. Additionally, each observational survey and age estimation technique has its own systematics, and no attempt has been made to characterize such systematics, and we also address this issue.

1.3 Disc evolution in the age of massive galactic surveys

A number of large observational surveys cataloguing the detailed properties of a huge numbers of stars in the Milky Way mean that we are better poised now than ever before to unravel the fundamental velocity dispersion relations. These data sets probe stellar kinematics well beyond the solar neighbourhood, and hence provide more coverage of the angular momentum and metallicity dimensions. Additionally, these data sets have large sample of stars that allows the additional dependence on metallicity and angular momentum to be studied robustly. The combination of *Gaia* DR2 astrometry and accurate radial velocities from ground-based spectroscopic surveys provides precise six-dimensional phase-space information for a large number of stars. Spectroscopic surveys such as GALAH and LAMOST, mean that it is now possible to get reliable age estimates for a large number of main sequence turn-off (MSTO) and subgiant stars in the solar neighbourhood, a significant improvement when compared with photometry-based ages (e.g. Bland-Hawthorn et al. 2019). Asteroseismology from missions like *Kepler* and *K2* has opened the door to estimating the ages of intrinsically bright giant stars, allowing us to study the velocity dispersions well beyond the solar neighbourhood. Ground-based spectroscopic surveys also provide elemental abundances, with which we can tag stellar populations that were born at the same time and same place (Freeman & Bland-Hawthorn 2002).

Some attempts have already been made to characterize the velocity dispersions, using the large observational surveys that probe the velocity dispersion beyond the solar neighbourhood and below we summarize four such studies. Sanders & Das (2018) used data from multiple observational surveys and multiple stellar types (about 1.2 million stars), but did not consider potential systematics between the different surveys used. They studied the dependence of velocity dispersion on age and radius R, but ignored the dependence on angular momentum, metallicity, and z. They found that velocity dispersion decreases exponentially with R out to the solar Galactic radius and that beyond this σ_z tends to increase, while σ_R tends to flatten out. The velocity dispersion was found to grow as a power law with age, with exponent $\beta_R \sim 0.3$ and $\beta_z \sim 0.4$.

Ting & Rix (2019) and Mackereth et al. (2019) both studied the relationship between age and kinematics using APOGEE-DR14 data and ages estimated using a neural network model, which was trained on asteroseismic ages from the NASA *Kepler* mission. Ting & Rix (2019) used a sample of about 20 000 red clump stars, while Mackereth et al. (2019) used a sample of about 65 000 giants. Ting & Rix (2019) studied the dependence of the expectation value of the vertical action $\hat{J}_z$ as a function of age and average radius $\overline{R}_{\rm GC}$, which was defined to be the mean of the birth radius and the current radius. Crucially, they did not consider the dependence on birth radius and angular momentum separately, and also they did not study the in-plane kinematics. They found that the expectation value of birth action $\hat{J}_{z,0}$ is constant until about $\overline{R}_{\rm GC} = 10$ kpc but rises beyond that. Assuming the following approximate relations, which are valid under epicycle approximation, $\hat{J}_z \propto \sigma_z^2/\nu$, and $\nu \propto \sqrt{\Sigma}$, where ν is vertical oscillation frequency and Σ is mass surface density, we interpret their results as follows. The vertical dispersion falls off exponentially with $\overline{R}_{GC}$ until 10 kpc, but beyond that it flattens or increases. They also found that the vertical dispersion increases with age as a power law with exponent β_z ranging from 0.5 to 0.65.

Mackereth et al. (2019) studied the velocity dispersion as a function of Galactocentric cylindrical coordinates R and z for stars binned by age, [Fe/H] and [α/Fe]. A quadratic model was assumed for dependence on z, and an exponential model for dependence on R. We note that the exponential model might be inappropriate, given that Sanders & Das (2018) find the dependence of dispersion on R to be exponential only for $R < 8$ kpc, but flat and even rising for $R > 8$ kpc. Mackereth et al. (2019) found that for young stars the dispersions and the ratio σ_z/σ_R increase with height $|z|$, which they attribute to stronger heating by spiral structure in the plane and the relatively longer time-scale for GMCs to redirect random in-plane motion to vertical motion. For a given age, they find that the dispersions are higher for those mono-metallicity populations that have a larger mean orbital radius. But given that they study their stars by binning them up in mono-metallicity populations and the fact that metallicity is anticorrelated with mean orbital radius, we note that the observed trend with mean orbital radius is indistinguishable from a trend with metallicity.

Minchev et al. (2018) studied the vertical dispersion σ_z, of about 500 solar-neighbourhood stars as a function of birth radius and age. The dependence of σ_z on angular momentum was not studied. For a given age, the σ_z was found to vary with birth radius such that it has a slope, which is positive for old stars (age greater than 8 Gyr), flat for intermediate-age stars, and slightly negative for young stars (age less than 4 Gyr).

2 DATA

In this paper, we mainly make use of data from the LAMOST (Deng et al. 2012; Zhao et al. 2012) and GALAH spectroscopic survey (De Silva et al. 2015). We also use the APOGEE-DR14 spectroscopic survey (Majewski et al. 2017), but only for the purpose of studying systematic effects. We used the LAMOST-DR4 value added catalogue from Xiang et al. (2017b), for radial velocity, $T_{\rm eff}$, $\log g$, [Fe/H], [α/Fe], and distance. For LAMOST stars, we used two types of stars, the MSTO stars and the red-giant (RG) stars. The ages for the LAMOST-MSTO sample were taken from Xiang et al. (2017a) and for the LAMOST-RG-CN sample were taken from Wu et al. (2019). The LAMOST-RG-CN sample consists only of red giant branch stars (red clump stars are not included), with ages derived from spectroscopic C and N features. For the GALAH survey, we also used two types of stars, the MSTO stars and the RG stars. More precisely, we make use of the extended GALAH+ DR3 catalogue by Buder et al. (2021), which also includes data from TESS-HERMES (Sharma et al. 2018) and K2-HERMES (Sharma et al. 2019) surveys that use the same spectrograph and observational set-up as the GALAH survey. The RG stars that we use have asteroseismic information from the NASA K2 mission and their spectroscopic follow-up was done by the K2-HERMES survey, hereafter they are referred to as GALAH-RG-K2.

To select stars with reliable ages, we adopt the following selection function for MSTO stars,

$$(3.2 < \log g < 4.1)\&(5000 < T_{\rm eff}/{\rm K} < 7000). \quad (1)$$

Downloaded from https://academic.oup.com/mnras/article/506/2/1761/6307041 by INAF Trieste (Osservatorio Astronomico di Trieste) user on 13 April 2022

Table 1. Description of the different data sets used to study velocity dispersion.

Name	Spectroscopic survey	Stellar type	Asteroseismology	Age estimation	Stars
LAMOST-MSTO	LAMOST-DR4	MSTO		Xiang et al. (2017a)	398,173
LAMOST-RG-CN	LAMOST-DR4	red-giant-branch		Wu et al. (2019)	326,606
GALAH-MSTO	GALAH-iDR3	MSTO		BSTEP (Sharma et al. 2018)	101,328
GALAH-RG-K2	GALAH-iDR3	red-giant	K2-CAN	BSTEP (Sharma et al. 2018)	6,445
APOGEE-RG-KEPLER	APOGEE-DR14	red-giant	*Kepler*-CAN	BSTEP (Sharma et al. 2018)	6,091

For the RG stars, we adopt the following selection criteria,

$$(1 < \log g < 3.5)\&(3500 < T_{\rm eff}/{\rm K} < 5500). \quad (2)$$

The ages and distances for the GALAH-MSTO and GALAH-RG-K2 stars are computed with the BSTEP code (Sharma et al. 2018). BSTEP provides a Bayesian estimate of intrinsic stellar parameters from observed parameters by making use of stellar isochrones. For results presented in this paper, we use the PARSEC-COLIBRI stellar isochrones (Marigo et al. 2017). For the GALAH-MSTO stars, we use the following observables, $T_{\rm eff}$, $\log g$, [Fe/H], [α/Fe], J, Ks and parallax. For the GALAH-RG-K2 stars, in addition to the above observables, we use the asteroseismic observables $\Delta\nu$ and $\nu_{\rm max}$. These stars were observed by the NASA K2 mission as part of the K2GAP programme (Stello et al. 2015) and includes stars from campaigns 1 to 15. The asteroseismic analysis is conducted with the method by Kallinger et al. (2010), Kallinger et al. (2014), known as the CAN pipeline. $\Delta\nu$ and $\nu_{\rm max}$ for the model stars in the isochrones are determined with the ASFGRID code Sharma et al. (2016) that incorporates corrections to the $\Delta\nu$ scaling relation suggested by stellar models. A summary of different data sets used in this paper is given in Table 1.

Transformation from heliocentric to Galactocentric coordinates is done assuming $R_\odot = 8.0$ kpc (Reid 1993), $z_\odot = 0.025$ kpc, $\Omega_\odot = 30.24$ km s^{-1} kpc^{-1} (Reid & Brunthaler 2004), $U_\odot = 10.96$ km s^{-1} and $W_\odot = 7.53$ km s^{-1} (Sharma et al. 2014). We use a right-handed UVW coordinate system, where U points towards the Galactic centre, V is in the direction of the Galactic rotation, and W points towards the North Galactic pole. The transformation is carried out with the following heliocentric quantities: *Gaia* DR2 angular position and proper motions, spectroscopic radial velocities, and spectro-photometric distances. Where needed we assume the circular velocity at Sun, $\Theta_\odot$, to be 232 km s^{-1} (Sharma et al. 2014).

3 METHOD

3.1 Modelling the velocity dispersion

The dispersion σ_v of velocity v (for either v_R or v_z) is assumed to depend on the stellar age τ, angular momentum L_z, metallicity [Fe/H], and vertical height from the disc mid-plane z, via the following multiplicatively separable functional form

$$\sigma_v(X, \theta_v) = \sigma_v(\tau, L_z, [{\rm Fe/H}], z, \theta_v) = \sigma_{0,v} f_\tau f_{L_z} f_{[{\rm Fe/H}]} f_z. \quad (3)$$

Here, $X = \{\tau, L_z, [{\rm Fe/H}], z\}$ is a set of observables that are independent variables and

$$f_\tau = \left(\frac{\tau/{\rm Gyr} + 0.1}{10 + 0.1}\right)^{\beta_v}, \quad (4)$$

$$f_{L_z} = \frac{\alpha_{L,v}(L_z/L_{z,\odot})^2 + \exp[-(L_z - L_{z,\odot})/\lambda_{L,v}]}{1 + \alpha_{L,v}}, \quad (5)$$

$$f_{[{\rm Fe/H}]} = 1 + \gamma_{[{\rm Fe/H}],v}[{\rm Fe/H}], \quad (6)$$

$$f_z = 1 + \gamma_{z,v}|z|, \quad (7)$$

and $\theta_v = \{\sigma_{0,v}, \beta_v, \lambda_{L,v}, \alpha_{L,v}, \gamma_{[{\rm Fe/H}],v}, \gamma_{z,v}\}$ is a set of free parameters. The reasons behind the choice of the independent variables τ, L_z and [Fe/H] are discussed in Section 1.2, while the choice of $|z|$ was based on findings of Mackereth et al. (2019). The functional forms were chosen based on a preliminary analysis of the trends with respect to each observable. The σ_v has a power-law dependence on age, with β_v denoting the exponent. The age relation has a finite birth dispersion for stars younger than 0.1 Gyr. The σ_v falls off exponentially with L_z with scale $\lambda_{L,v}$, but at large L_z it is allowed to rise as L_z^2 (to account for flaring) and this rise is controlled by $\alpha_{L,v}$. The σ_v varies linearly with both [Fe/H] and $|z|$ with gradients $\gamma_{[{\rm Fe/H}],v}$ and $\gamma_{z,v}$, respectively. The $\sigma_{0,v}$ is a constant that denotes the velocity dispersion for stars lying in the mid-plane with solar metallicity, solar angular momentum ($L_{z,\odot} = \Omega_\odot R_\odot^2$), and an age of 10 Gyr. The likelihood of the observed velocities $v = \{v_0, ...v_N\}$ for a sample of N stars can be written as

$$p(v_0, ..v_N|X_0, ..., X_N, \theta_v) = \prod_i \mathcal{N}(v_i|0, \epsilon_{vi}^2 + \sigma_v^2(X_i, \theta_v)), \quad (8)$$

with ϵ_{vi} being the uncertainty corresponding to the observed velocity v_i of the ith star. Here, $\mathcal{N}(v|\mu, \sigma^2) = \exp[-(v - \mu)^2/(2\sigma^2)]/\sqrt{2\pi\sigma^2}$ denotes the distribution of a random variable v sampled from a normal distribution with mean μ and variance σ^2. We find the maximum likelihood estimate (MLE) of θ_v by using the Nelder-Mead algorithm as implemented in the python package `scipy.optimize.minimize`. The MLE values of θ_v for the velocity components v_z and v_R are given in Table 2. Also given alongside are uncertainties, which were estimated using bootstrapping. The data used for estimating θ_v contained an equal number of stars from the LAMOST and GALAH surveys.

3.2 Visualizing the multivariate velocity dispersion

The velocity dispersions of stars in the Milky Way depend on multiple independent variables. To visualize the dependence of the velocity dispersion with respect to an independent variable x, we must divide out the dependence on other independent variables in the set X. We accomplish this by binning the stars in x and computing the dispersion of $v/\sigma_{v,[x]}$ in each bin to get a profile of the dispersion as a function of x. Here, $\sigma_{v,[x]}$, defined as

$$\sigma_{v,[x]}(X, \theta_v) = \sigma_{0,v} \prod_{y \in X}^{x \neq y} f_y(y|\theta_v), \quad (9)$$

is the complementary velocity dispersion that includes all independent variables in set X except x.

Downloaded from https://academic.oup.com/mnras/article/506/2/1761/6307041 by INAF Trieste (Osservatorio Astronomico di Trieste) user on 13 April 2022

Table 2. MLEs of parameters θ_v used to model the dispersion of velocity components v_z and v_R.

v	$\sigma_{0,v}$	β_v	$\lambda_{L,v}$	$\alpha_{L,v}$	$\gamma_{[\mathrm{Fe/H}],v}$	$\gamma_{z,v}$
v_z	21.1 ± 0.2 km s^{-1}	0.441 ± 0.007	1130 ± 40 kpc km s^{-1}	0.58 ± 0.04	-0.52 ± 0.01 km s^{-1} dex^{-1}	0.20 ± 0.01 km s^{-1} kpc^{-1}
v_R	39.4 ± 0.3 km s^{-1}	0.251 ± 0.006	2300 ± 200 kpc km s^{-1}	0.09 ± 0.04	-0.19 ± 0.01 km s^{-1} dex^{-1}	0.12 ± 0.01 km s^{-1} kpc^{-1}

4 RESULTS

4.1 Basic trends

Our basic trends with angular momentum, age, metallicity, and perpendicular distance from the plane are shown in Fig. 1. The top panels explore the vertical dispersion while the bottom panels explore the radial dispersion. The dispersion is assumed to be a function of multiple independent variables, and from left to right each panel shows the effect of one independent variable at a time. The dispersions decrease exponentially with L_z up to about the solar angular momentum, beyond that σ_z starts to increase (Fig. 1a) whereas σ_R flattens (Fig. 1e). The dispersions increase with age and are well described by a power law, with the exponent being higher for σ_z as compared to σ_R (Figs 1b and f). The GALAH-MSTO data set does not show any saturation for older stars, but other data sets show a flattening for stars older than 10 Gyr. The dispersions decrease linearly with both [Fe/H] (Figs 1c and g) and $|z|$ (Figs 1d and h), with the slope being steeper for σ_z. Fig. 2 demonstrates that all of the above discussed trends are independent of the location R and are valid for $3 < R/\mathrm{kpc} < 20$.

Data from different surveys and stellar types are shown separately in Fig. 1. Figs 1(a) and (b) show some systematic differences, but overall the different data sets are all found to be consistent with the same relationship. Agreement between the GALAH and LAMOST results suggests that their spectroscopic parameters do not have any strong systematics with respect to each other. Agreement between data sets of different stellar types (MSTO and RG) suggests there are no strong systematics related to stellar types. This is very reassuring and useful given the fact that for different stellar types very different age estimation techniques are used.

4.2 Variation of basic trends with respect to other independent variables

In Figs 3–11, we show the residual dependence of each relation on other independent variables. In each figure, we plot the observed relation corresponding to one independent variable, such as the relation f_τ, by binning stars in another independent variable, e.g. L_z or [Fe/H]. In general, we find that the basic shape of the relations vary very little with respect to other independent variables, suggesting that modelling the dispersion as a product of multiple independent functions, as given by equation (3), is a good approximation. However, this approximation is not perfect. The relations, when binned with respect to other variables, do show variations that are statistically significant. Interestingly, the variations that we see are in most cases systematic, which mean that in principle they can be accommodated by introducing more degrees of freedom in the model. The existence of these variations does not invalidate the fact that the dispersion can be expressed as a function of L_z, age, [Fe/H] and $|z|$; it only implies that the multiplicative separable form is not perfect. Below we discuss the variations in more detail.

The f_{L_z} relation varies with age such that the younger stars have higher relative dispersion (Fig. 3). Here, by relative dispersion, we mean dispersion relative to the derived relations. The f_{L_z} relation varies with [Fe/H], such that for high L_z, the metal-rich stars have systematically higher relative dispersion (Fig. 4). The f_τ relation does not vary for stars with age less than 8 Gyr, but for older stars the relative dispersion is systematically lower for the high-L_z stars (Fig. 5) and for high-metallicity stars (Fig. 6). This could be because both old high-L_z stars and old high-metallicity stars are rare and hence an old star bin is more likely to be contaminated by young stars (due to age uncertainties), which will lower the overall dispersion in that bin given that young stars have low dispersion.

The $f_{[\mathrm{Fe/H}]}$ relation flattens with increasing L_z (Fig. 7). The relation does not vary much with age, with the exception that for old stars the relative dispersion is lower at the high-metallicity end (Fig. 8). This again could be due to old and high-metallicity stars being rare and hence an old star bin is more likely to be contaminated by young stars. The f_z relation for vertical velocity dispersion does not seem to vary much with L_z (Fig. 9a); however, the f_z relation for radial velocity dispersion flattens with increase in L_z (Fig. 9b). The f_z relation does not vary much with age (Fig. 10) or [Fe/H] (Fig. 11). However, for stars younger than 4 Gyr the relationship is much steeper (Fig. 10).

4.3 Systematics between surveys

In Fig. 1, we presented results from four different data sets. Two were based on the LAMOST spectroscopic survey, with one made up of MSTO stars and other made up of RGB stars. The other two data sets were based on the GALAH spectroscopic survey, with one made up of MSTO stars and other of RG stars having asteroseismic information from K2. Another large spectroscopic survey that we did not use in Fig. 1 was APOGEE. In Fig. 12(a), we plot APOGEE results for the asteroseismic sample from *Kepler* (Pinsonneault et al. 2018). It shows that the observed AVR is shifted with respect to our empirical relations. Examination of stars in between the APOGEE and GALAH/LAMOST data sets, revealed that the APOGEE iron abundances were systematically higher by 0.1 dex. However, this is still not enough to account for the difference seen in Fig. 12(a). A further increase in the age of APOGEE stars by 10 per cent is required to bring the APOGEE-RG-KEPLER data set into agreement with the other data sets. These systematic offsets are the reason APOGEE data was not used in the analysis presented in Fig. 1. Fig. 12(b) shows that with these changes the APOGEE-RG-KEPLER data set can also be brought into agreement with the GALAH-RG-K2 data.

In Fig. 1, the LAMOST-MSTO and LAMOST-RG-CN data sets show significant flattening of the AVR for age greater than 10 Gyr, while such a flattening is not seen for the GALAH-MSTO stars. The flattening for LAMOST data sets could be due to larger uncertainties on age estimates in them. Fig. 12(c) shows results for the LAMOST-MSTO and LAMOST-RG-CN data sets, using age estimates from Sanders & Das (2018). No flattening is seen here. This could be because the Sanders & Das (2018) ages are more precise than LAMOST ages for the older stars. However, it should be noted that Sanders & Das (2018) use strong priors based on height above the plane, which can increase the age precision for older stars, but is not

Downloaded from https://academic.oup.com/mnras/article/506/2/1761/6307041 by INAF Trieste (Osservatorio Astronomico di Trieste) user on 13 April 2022

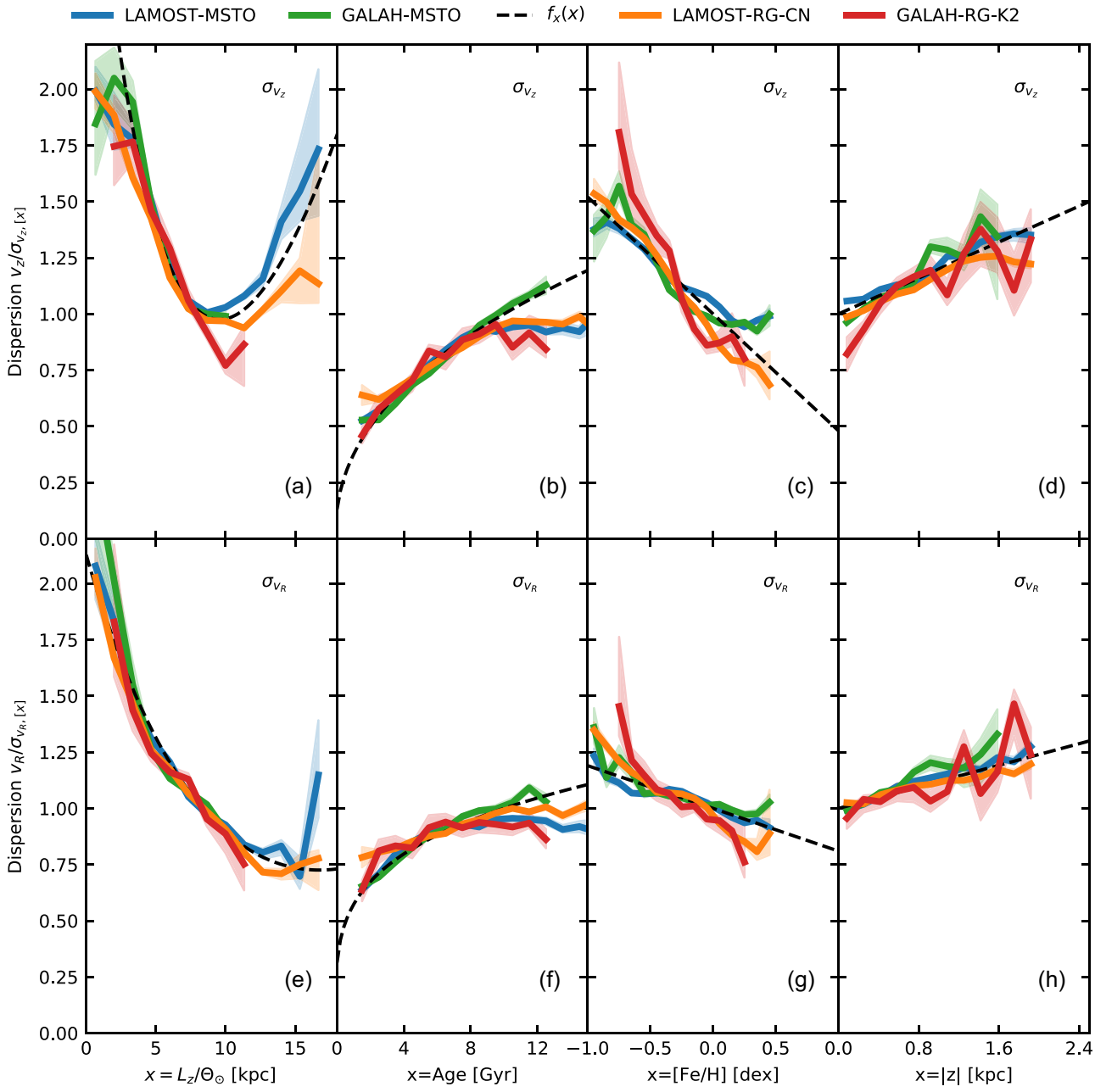

Figure 1. Velocity dispersion as a function of angular momentum, age, metallicity, and height above the Galactic mid-plane for different data sets. The shaded region denotes the 16 and 84 percentile confidence interval estimated using bootstrapping. The velocity dispersion is modelled as $\sigma = \sigma_0 f_\tau f_{L_z} f_{[\mathrm{Fe/H}]} f_z$. Panels from left to right show the dispersion of $v/\sigma_{v,[L_z]}$, $v/\sigma_{v,[\tau]}$, $v/\sigma_{v,[\mathrm{Fe/H}]}$, and $v/\sigma_{v,[z]}$ respectively, for the observed stars. $\sigma_{v,[x]}$ is an analytical function as given by equation (9) and is designed to divide out the dependence of variables other than x (see Section 3.2). The top panels show the dispersion in vertical velocity v_z, while the bottom panels show the dispersion in Galactocentric radial velocity v_R. The dashed lines show the best-fitting model profiles based on equation (3) and parameters given in Table 2.

ideal to study trends with height above the plane, as we do in this paper.

4.4 The role of angular momentum in shaping the solar-neighbourhood AVR

Angular momentum plays a critical role in shaping the AVR of stars observed in the solar neighbourhood. Here, we are talking about AVR, which is marginalized over other variables like angular momentum and [Fe/H]. It has been claimed in some previous studies that the AVR deviates from a power law with an abrupt increase for old stars (Freeman 1991; Edvardsson et al. 1993; Quillen & Garnett 2001). Since, most old stars in the solar neighbourhood belong to the thick disc, this tentatively suggests that the kinematics of the thick disc stars is different from that of the thin disc stars. We show in Fig. 13 that this apparent break is due to a systematic variation of angular momentum with age, since older stars have low angular momentum and low angular momentum stars have higher velocity dispersion. Once again, when a variation due to angular momentum is divided out, all stars seem to be consistent with a

Downloaded from https://academic.oup.com/mnras/article/506/2/1761/6307041 by INAF Trieste (Osservatorio Astronomico di Trieste) user on 13 April 2022

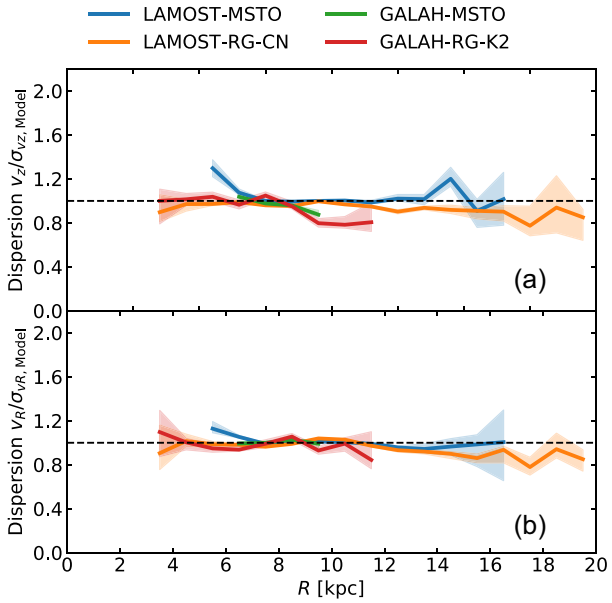

Figure 2. Dispersion of normalized velocity as a function of Galactocentric radius R. The shaded region denotes the 16 and 84 percentile confidence interval estimated using bootstrapping. The velocity is normalized by dividing with the velocity dispersion predicted by the model $\sigma_v(X, \theta_v)$ as given by equation (3). The dashed line corresponds to the expected value of 1 for the case where the model describes the data perfectly.

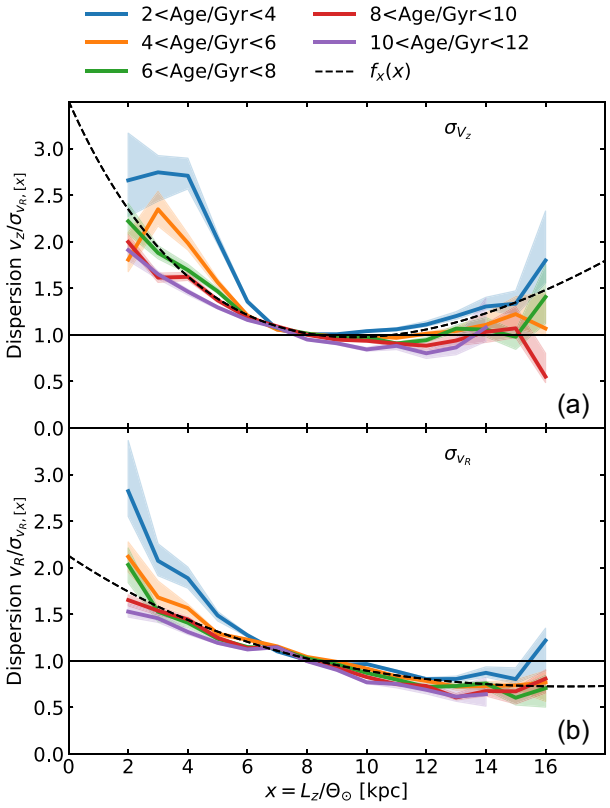

Figure 3. Velocity dispersion as a function of angular momentum for stars lying in different age bins. The shaded region denotes the 16 and 84 percentile confidence interval. The dependence on other independent variables (age, [Fe/H], and $|z|$) have been divided out (see Section 3.2). The observed stars are from LAMOST-MSTO, LAMOST-RG-CN, GALAH-MSTO, and GALAH-RG-K2 data sets. The dashed lines show the the best-fitting model profiles. The curves are normalized to have unit dispersion at $L = \mathrm{L}_\odot$. The profiles do not show any significant variation with the age. The profile for the youngest bin is slightly steeper.

universal AVR (green line in Fig. 1). Hence, the AVR of stars in the solar neighbourhood is an example of Yule-Simpson's paradox, an apparent relationship due to incorrect statistical modelling. A detailed discussion of Yule-Simpson's paradox in the context of Galactic archaeology is given by Minchev et al. (2019). Finally, it is still not clear as to why the angular momentum decreases with age. It could be due to inside out formation of the disc and radial migration of stars from the inner disc and needs to be investigated in future.

5 DISCUSSIONS

5.1 Dependence of dispersions on age

We find $\beta_z = 0.44$ and $\beta_R = 0.26$, which is in good agreement with predictions of simulations by Aumer et al. (2016a), where the effects of spiral arms, GMCs and a bar is taken into account. For the GALAH-MSTO stars, even the old thick disc stars satisfy this relationship. The LAMOST-MSTO, LAMOST-RG-CN, and GALAH-RG-K2 all show saturation for age greater than 10 Gyr. This could be due to significant uncertainties in ages for the older stars in samples other than GALAH-MSTO (see e.g. Martig, Minchev & Flynn 2014). Our giant samples make use of asteroseismology to determine ages. The uncertainty of asteroseismic ages is known to increase with age and is predicted to be around 30 per cent for RGB stars and even higher for red-clump stars (Silva Aguirre et al. 2018). Since old stars are typically rare, an old star bin is more likely to be contaminated by young stars (due to age uncertainties), which will lower the overall dispersion in that bin given that young stars have low dispersion.

As discussed in Aumer et al. (2016a), the exponents β_z and β_R of the AVR depend in a complex way upon the whole dynamical history of the Galaxy. This is because there are at least two major scattering agents (spiral structures and GMCs) and the strength of scattering due to them changes with time. Spiral structure is mainly responsible for in-plane scattering, while GMCs contribute to both in-plane and vertical scattering. Spiral structure drives up σ_R fairly rapidly, increasing the Toomre stability parameter Q and making the disc stable. This makes the ratio σ_z/σ_R very small initially. Thereafter, on a longer time scale, scattering from GMCs increases both σ_R and σ_z. For scattering from stationary fluctuations, the exponent β is predicted to be around 0.25, with β_z being slightly higher than β_R (Hänninen & Flynn 2002). This is seen in the heating history of coeval populations. However, β_z for the AVR is much higher because the overall efficiency of heating due to GMCs is higher at earlier times (fig. 7 of Aumer et al. 2016a). At earlier times, the star formation rate is high and the stellar disc mass is low and this makes the GMC mass fraction higher, which in turn increases the efficiency of GMC scattering.

5.2 Dependence of dispersions on angular momentum

Without any loss of generality, in what follows, we discuss our results in terms of guiding radius rather than angular momentum, with the guiding radius being defined as $R_g = L_z/\Theta_\odot$ (angular momentum divided by circular velocity at Sun). We find that for $R_g < \mathrm{R}_\odot$ both dispersions fall off exponentially with R_g. In general, the strength of the secular heating processes, like those due to spiral arms or

Downloaded from https://academic.oup.com/mnras/article/506/2/1761/6307041 by INAF Trieste (Osservatorio Astronomico di Trieste) user on 13 April 2022

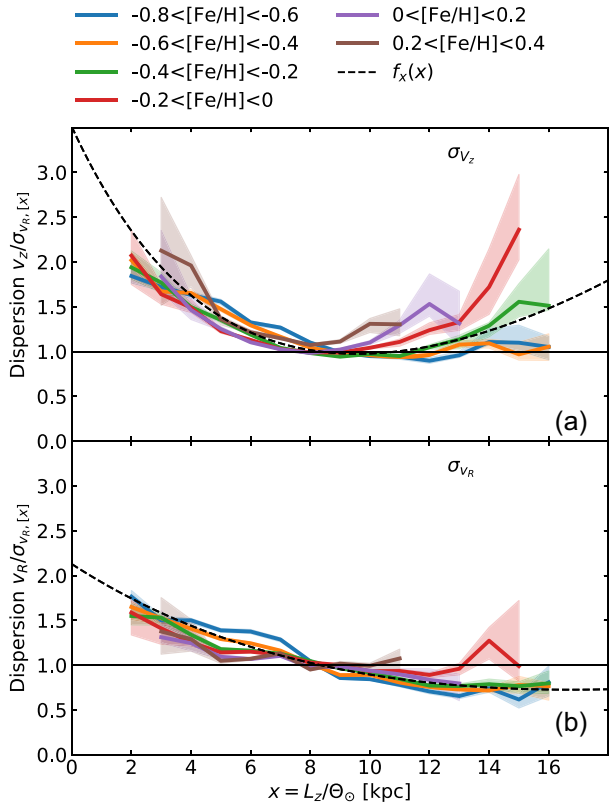

Figure 4. Same as Fig. 3 but for stars lying in different [Fe/H] bins. The vertical dispersion is slightly higher for metal rich stars.

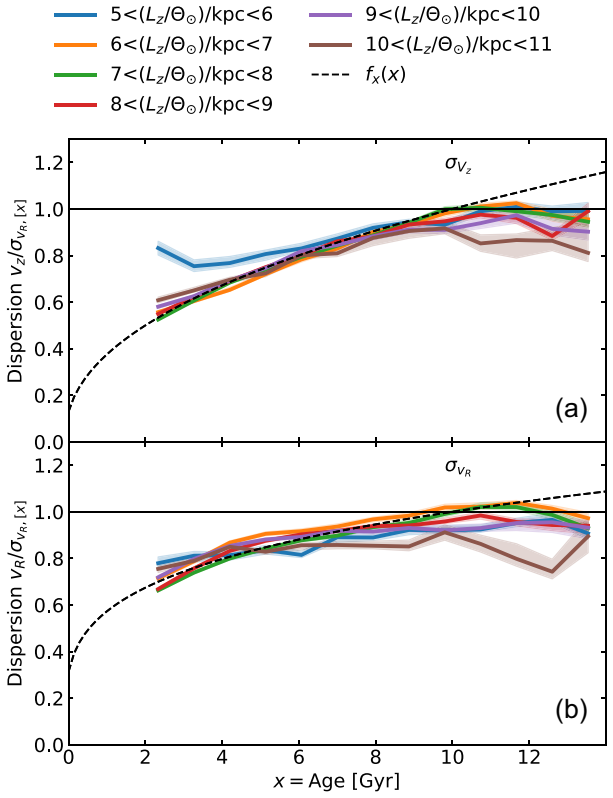

Figure 5. Velocity dispersion as a function of age for stars lying in different L_z bins. The shaded region denotes the 16 and 84 percentile confidence interval. The curves are normalized to have unit dispersion at an age of 10 Gyr. The dependences on other independent variables (L_z, [Fe/H], and $|z|$) have been divided out (see Section 3.2). The description of the panels and the data set used are same as in Fig. 3. For older stars, the profiles show a mild variation with L_z.

GMCs, are expected to be proportional to the surface density of stars Σ, so the dispersion is expected to fall off with radius. Using some simple physically motivated arguments we now predict the radial scale length R_σ of the exponential fall of dispersion with R. The vertical dispersion is expected to vary with surface density Σ, and scale height h_z, as $\sigma_z \propto \sqrt{\Sigma h_z}$ (van der Kruit 1988). If h_z is constant then the scale length of vertical dispersion, R_{σ_z}, should be related to the scale length of stellar surface density, R_d, as $R_{\sigma_z} = 2R_d$. Using this we estimate $R_{\sigma_z} = \lambda_{L,v_z}/\Theta_\odot = 4.9 \pm 0.2$ kpc (adopting $\Theta_\odot = 232$ km s^{-1} from Sharma et al. 2014), which is in good agreement with the theoretical prediction of 5.0 kpc (adopting $R_d = 2.5$ kpc, see e.g. Robin et al. 2003; Jurić et al. 2008). For the radial dispersion we expect $\sigma_R \propto \Sigma R$ and hence $R_{\sigma_R} = R_d$. This follows from assuming the Toomre stability parameter

$$Q = \frac{\sigma_R \kappa}{3.36 G \Sigma} \tag{10}$$

to be constant throughout the disc and the rotation curve to be flat, which implies $\kappa \propto 1/R$. However, we find R_{σ_R} to be 9.9 kpc, which is about four times larger than R_d (assuming $R_d = 2.5$ kpc). Hence, the observed scale length of σ_R cannot be explained by a constant Q.

For $R_g > R_\odot$ kpc, both dispersions break away from being purely exponential functions of R_g, with σ_z increasing and σ_R flattening with R_g. From previous discussion we know that the disc will flare if σ_z falls off slower than $\sqrt{\Sigma}$, remains flat, or rises. Hence, the observed behaviour of σ_z will flare the outer disc for mono-age and mono-metallicity populations. Minchev et al. (2015) argue on theoretical grounds that flaring of mono age populations is almost inevitable in disc galaxies, while the overall disc can still have little or no flaring. In the Milky Way, outside the solar radius significant flaring has been reported for all mono age populations, with the flaring being strongest for the youngest population (Mackereth et al. 2017). This is consistent with our overall reported rise of σ_z with R_g in the outer disc, and also the stronger rise of σ_z for younger stars as shown in Fig. 3.

The flattening of velocity dispersion with R_g is easy to understand. Stars are thought to be born out of the inter-stellar medium with a birth dispersion of about 10 km s^{-1}, due to turbulence in the medium driven by the injection of energy from newly forming stars. Due to this non-zero lower bound on the dispersion of newly forming stars, at large R_g the dispersion cannot keep on falling exponentially but will hit a floor and flatten.

We see in Figs 1(b) and (d) that the flattening occurs at a smaller value of R_g for σ_z as compared to σ_R. This is also easy to understand. Both σ_z and σ_R are exponential functions of R_g, but the overall proportionality constant for σ_R is larger than σ_z. Additionally, the scale length for σ_R is larger than that for σ_z. Consequently, flattening due to a constant birth dispersion will set in at a lower value of R_g for σ_z than for σ_R. The youngest stars also have the lower overall proportionality constant for dispersion, so they are expected to flatten earlier and this is visible in Fig. 3. The fact that non-zero birth dispersion can lead to flattening of dispersions and consequently flaring has been nicely demonstrated by Aumer, Binney & Schönrich (2016b), using N-body simulations of discs having spiral arms, GMCs, and a bar.

What causes the dispersions to rise for σ_z and why does not it also rise for σ_R? This needs to be investigated in future. Simulations by

Downloaded from https://academic.oup.com/mnras/article/506/2/1761/6307041 by INAF Trieste (Osservatorio Astronomico di Trieste) user on 13 April 2022

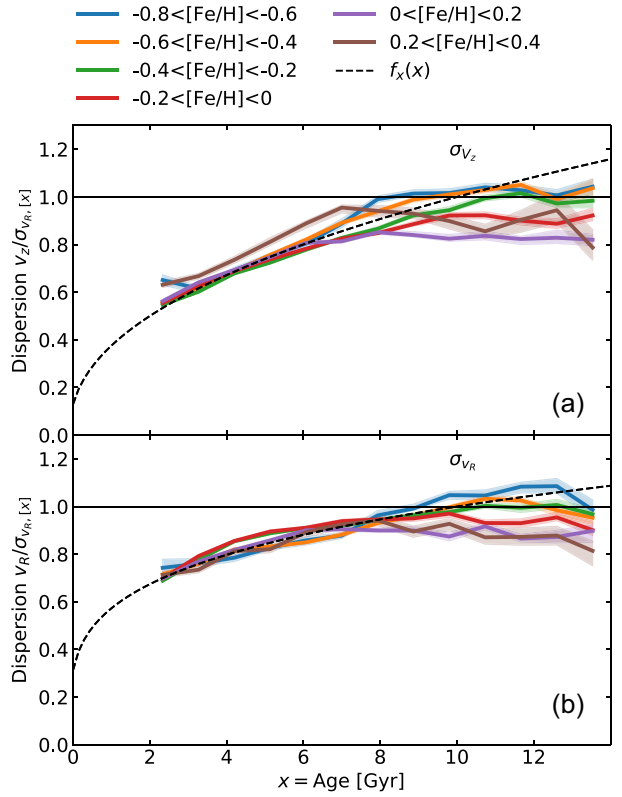

Figure 6. Same as Fig. 5 but for stars lying in different [Fe/H] bins. For older stars the profiles show a mild variation with [Fe/H].

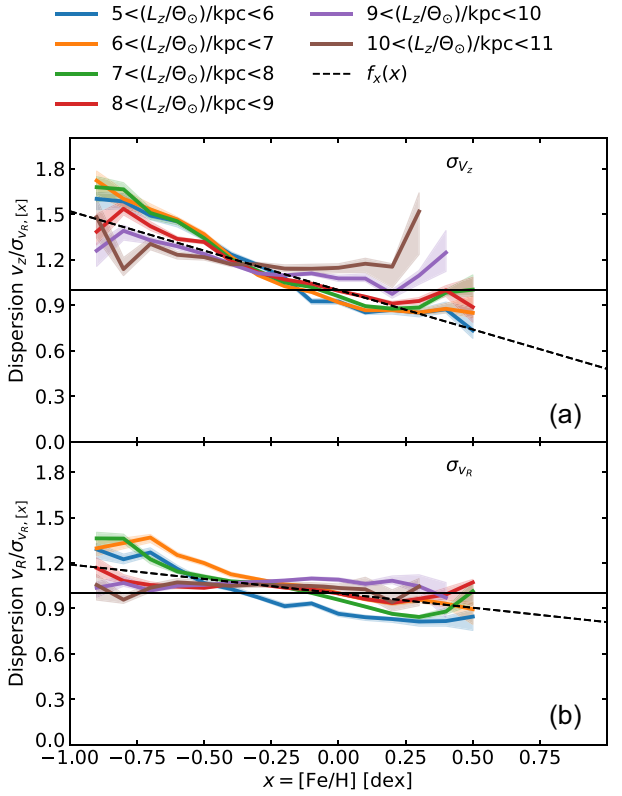

Figure 7. Velocity dispersion as a function of metallicity, [Fe/H], for stars lying in different angular momentum bins. The shaded region denotes the 16 and 84 percentile confidence interval. The curves are normalized to have unit dispersion at [Fe/H] = 0. The dependence on other independent variables (L_z, age, and $|z|$) have been divided out (see Section 3.2). The description of the panels and the data set used are same as in Fig. 3. The profiles show a mild variation with L_z, with the profiles becoming flatter with increase of L_z.

Aumer et al. (2016a), incorporating the effects of spiral perturbations, a bar, and GMCs, only predict a monotonic fall or flattening for σ_z, but no rise of dispersion with radius (see their fig. 4). This suggests that some additional processes might be at play. Three good candidates are processes listed by Minchev et al. (2015) in the context of flaring. For example, the interaction of the disc with orbiting satellites (Kazantzidis et al. 2008; Villalobos & Helmi 2008; Bournaud, Elmegreen & Martig 2009) is known to cause flaring in the outer disc. The infall of misaligned gas (Roškar et al. 2010; Sharma, Steinmetz & Bland-Hawthorn 2012; Aumer et al. 2013) and reorientation of the disc axis (Aumer & White 2013) is also known to cause warps and consequently flaring. All of them can lead to increase of σ_z with R_g or R. The basic idea being that the outer disc, due to lower vertical restoring force, is more susceptible to external perturbations. Minchev, Chiappini & Martig (2014a), using a cosmological simulation, demonstrated that orbiting satellites lead to rise of σ_z with R. Later, Grand et al. (2016) showed that one of the disc galaxies (Au18) simulated in a cosmological context had a rise of σ_z with R. As this simulation did not have GMCs, Grand et al. (2016) attributed the vertical heating with radius to the bar and the effect of orbiting satellites.

5.3 The shape of the velocity ellipsoid

Our best-fitting relations (see equation (3) and Table 2) can be used to estimate the ratio σ_z/σ_R. These relations suggest that there is a strong dependence of the ratio σ_z/σ_R on age, metallicity, angular momentum, and height above the plane and this is shown in Fig. 14. More precisely, for 10 Gyr-old stars that are in the plane and have solar metallicity, the ratio first decreases with guiding radius to a minimum of 0.53 at $R_g = 7.25$ kpc, and then increases with R_g. The ratio is greater than 0.7 for $R_g > 12.0$ kpc. Also, the ratio increases monotonically with decrease in metallicity and increase of height. If the vertical velocity dispersion is governed by scattering from GMCs, an equilibrium ratio of 0.62 is predicted, which can be attained by relatively old stars that had enough time to scatter. Simulations by Aumer et al. (2016a) also suggest that spiral perturbations and GMCs can only lead to ratios σ_z/σ_R in range 0.5 to 0.7. But the fact that we find σ_z/σ_R to be greater than 0.7 in certain regions of the disc indicates that processes other than spiral structure and GMCs could be affecting the vertical dispersion of stars there.

5.4 Dependence of dispersions on metallicity

We see that velocity dispersions increase with decreasing metallicity for any given age and angular momentum (Figs 7 and 8). Our current understanding of disc formation suggests that the ISM probably had a negative metallicity gradient for a significant fraction of its lifetime (Schönrich & Binney 2009; Minchev et al. 2018). This suggests that at any given age the metallicity should decrease with the birth radius of a star. Consequently, velocity dispersions should increase with birth radius. This result is counter intuitive, as naively we expect the dispersion to decrease with any type of radius (Section 5.2). Interestingly and importantly, we observe the dispersions to increase with birth radius for stars of all ages and angular momentum.

One reason for the increase of dispersion with birth radius could be the conservation of vertical action, which will happen for stars of any

Downloaded from https://academic.oup.com/mnras/article/506/2/1761/6307041 by INAF Trieste (Osservatorio Astronomico di Trieste) user on 13 April 2022

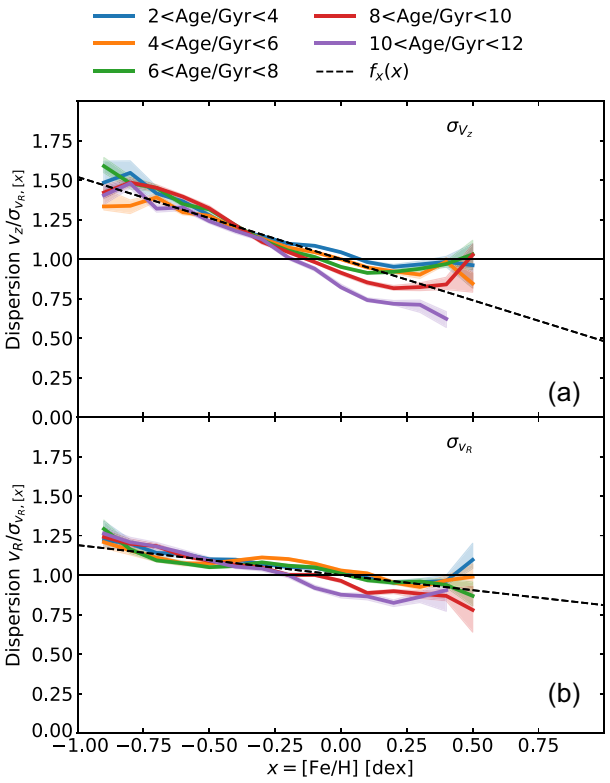

Figure 8. Same as Fig. 7 but for stars lying in different age bins. The profiles show a mild variation with the age, with the profiles becoming steeper with the increase of age.

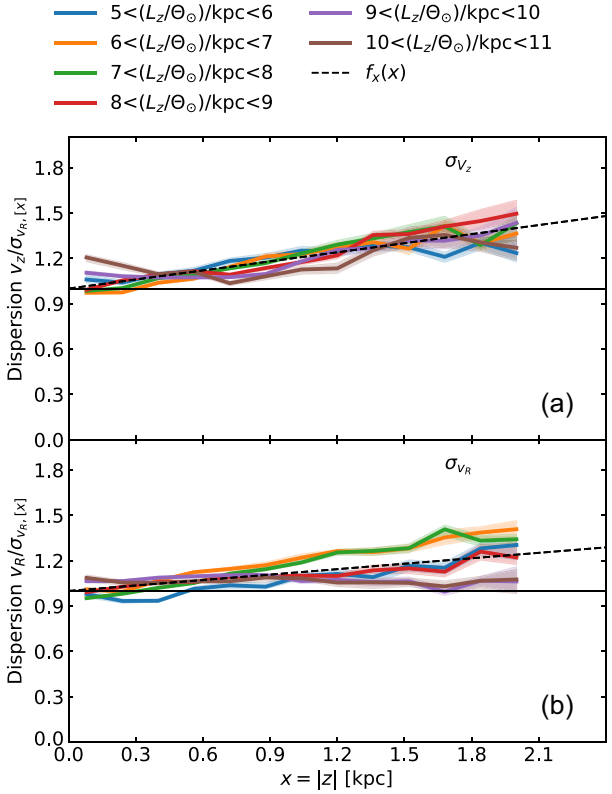

Figure 9. Velocity dispersion as a function of distance |z| from the mid-plane of the Galaxy, for stars lying in different angular momentum bins. The shaded region denotes the 16 and 84 percentile confidence interval. The dependence on other independent variables (L_z, age, and [Fe/H]) have been divided out (see Section 3.2). The description of the panels and the data set used are same as in Fig. 3. The relationship for radial dispersion shows a mild variation with the L_z, with the slope becoming flatter with the increase of Lz.

age or angular momentum. Solway, Sellwood & Schönrich (2012) demonstrated that vertical action is conserved for migrating stars. This conservation of vertical action leads to adiabatic heating/cooling of stars moving inwards/outwards (Minchev et al. 2012). To demonstrate this, let E_z be the vertical energy, ν the vertical oscillation frequency, Σ the surface density and σ_z the vertical velocity dispersion. Using some standard assumptions and approximations it is easy to show that the vertical action $J_z = E_z/\nu = \sigma_z^2/\sqrt{2\pi G\Sigma}$ (for details, see Section 1.3 and Minchev et al. 2012). When action is conserved, $\sigma_z \propto \Sigma^{1/4}$. Hence, a stellar population born at radius R_b with vertical velocity dispersion at birth of $\sigma_{z,\,\mathrm{before}}$ after migrating to orbits with guiding radius R_g will end up with a dispersion σ_z given by

$$\sigma_z = \sigma_{z,\mathrm{before}} \exp\left(-(R_g - R_b)/4R_d\right), \tag{11}$$

where R_d is the scale length of surface density distribution. From this expression, it is easy to see that relative to the initial velocity dispersion before migration, stars after migrating outwards cool down while stars after migrating inwards heat up.

The question(s) we are interested in is: for stars with a given angular momentum and age, how does the dispersion vary with birth radius and is the dispersion of outward migrators higher or lower than that of inward migrators? The answer to this will depend on how the initial velocity dispersion before migration, $\sigma_{z,\,\mathrm{before}}$, varies with R_b in equation (11). Unfortunately, this is not well known. If σ_z is to increase monotonically with R_b then according to equation (11), $\sigma_{z,\,\mathrm{before}}$ must be either flat, rising or fall of slower than $\exp(-R_b/(4R_d))$. A natural choice for $\sigma_{z,\,\mathrm{before}}$ is equation (3). This is flat or rising for $R_b > \mathrm{R}_\odot$ as required, but falls of faster than $\exp(-R_b/(4R_d))$ (in fact it falls with a scale length of $2R_d$). Hence, if $\sigma_{z,\,\mathrm{before}}$ is indeed given by equation (3), then migrating stars should be preferentially of low vertical dispersion as suggested by some studies. Vera-Ciro et al. (2014) demonstrated using an idealized simulation of a galaxy with spiral arms that migrating stars are preferentially of low vertical dispersion, given that they spend more time in the plane (see also Daniel & Wyse 2018). This bias was also shown to be present for discs in cosmological simulations (Grand et al. 2016), which made it possible for the outward migrators at a given radius to be cooler compared to non-migrators. Other processes that induce flaring, like orbiting satellites, warps, the infall of misaligned gas and reorientation of the disc (Minchev et al. 2015), can also lead to an increase of dispersion with birth radius (Minchev et al. 2014a, b).

Minchev et al. (2018) had also reported an increase of vertical dispersion with birth radius. However, they found the effect to be most prominent for older stars. The slope of variation of dispersion with birth radius was found to be positive for stars older than 8 Gyr and then flatten to zero at 6 Gyr and eventually turn negative for stars younger than 4 Gyr. In contrast, we find the slope to be positive for all ages, and additionally we also find a positive slope for the radial velocity dispersion, which they did not study (Fig. 8). Mackereth et al. (2019) using mono age and mono metallicity populations reported an increase of vertical dispersion with mean orbital radius for low-[α/Fe] stars. For the radial dispersion they reported an increase with mean orbital radius only for stars younger than 4 Gyr. Given that mean orbital radius decreases monotonically with the metallicity for their populations, this means that their results can also be interpreted

Downloaded from https://academic.oup.com/mnras/article/506/2/1761/6307041 by INAF Trieste (Osservatorio Astronomico di Trieste) user on 13 April 2022

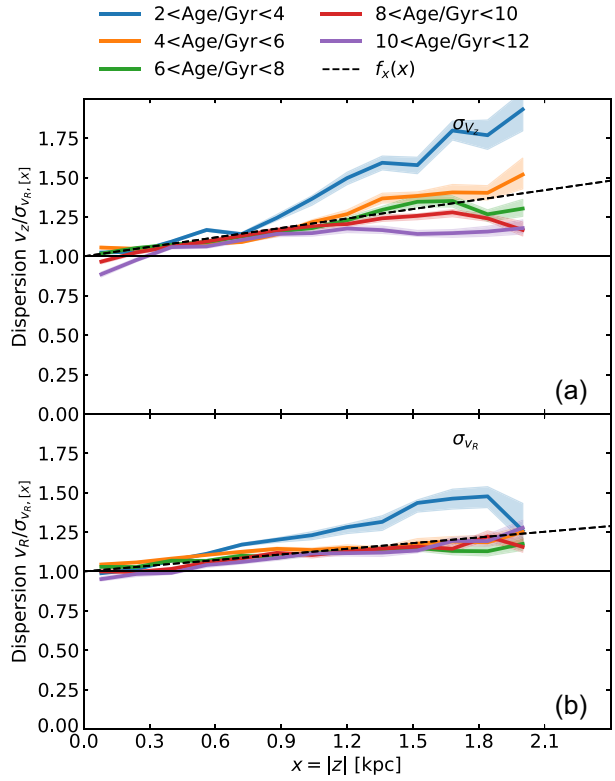

Figure 10. Same as Fig. 9 but for stars lying in different age bins. The slope is higher for younger stars.

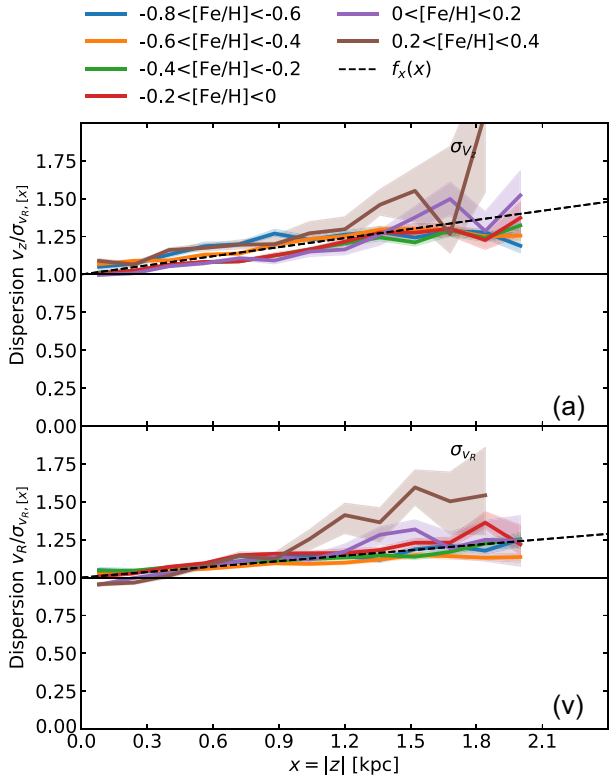

Figure 11. Same as Fig. 9 but for stars lying in different [Fe/H] bins. The relationship shows very little variation with [Fe/H].

as an increase of dispersion with birth radius. In that case, for stars younger than 4 Gyr the slopes are opposite of that of Minchev et al. (2018).

Importantly, both Minchev et al. (2018) and Mackereth et al. (2019) had not divided out the dependence on angular momentum, which can have the opposite effect, because for stars with angular momentum less than solar angular momentum, the dispersion increases with decrease of angular momentum. This could be responsible for the differences between the above studies and differences with the results presented here.

If [α/Fe] abundance is assumed to be a good proxy for age, then our metallicity (or birth radius) trends can also be considered to be consistent with the findings of Hayden et al. (2020). They studied the velocity dispersion as a function of [α/Fe] abundance in different [Fe/H] bins using GALAH-DR2 data. They found that the vertical dispersion increases with decrease of metallicity for any given [α/Fe] just as we find the same effect for any given age.

5.5 Dependence of dispersions on height

We find that velocity dispersions increase with height for all angular momentum (Fig. 9), ages (Fig. 10), and metallicities (Fig. 11). A positive slope is present for all ages but it is much steeper for stars younger than 4 Gyr (Fig. 10). Also the slope for σ_z is higher than that for σ_R by about a factor of 2. This suggests that the ratio of σ_z/σ_R also increases with height. A non-zero slope implies that the populations defined by a specific age and metallicity are non-isothermal. Mackereth et al. (2019) also report a positive slope for low [α/Fe] populations, which was found to flatten with age. For high-[α/Fe] populations the slope was found to be zero, whereas we find the high-[α/Fe] stars to have a positive slope. As suggested by Mackereth et al. (2019), the non-isothermality could be related to the relatively large time scale for GMC heating as compared to the relatively fast in-plane heating by spiral arms. This is something that can be easily tested in idealized simulations by Aumer et al. (2016a). However, as shown in van der Kruit (1988), isothermality is not necessary for constructing an equilibrium distribution. They show that for a self-gravitating disc whose vertical density distribution is exponential, the vertical dispersion is found to increase with $|z|$.

5.6 Dependence of dispersions on [α/Fe] abundance

Contrary to claims by Mackereth et al. (2019) that the velocity dispersion properties of the high-[α/Fe] population is different from that of the low-[α/Fe], we find very little difference between the two populations. We demonstrate this in Fig. 15, where we plot the dispersion as a function of various different independent variables. The dashed lines show the best-fitting relation obeyed by all stars, which can be considered as the relationship obeyed by low-[α/Fe] stars, as the sample of all stars is dominated by them. The high-[α/Fe] stars are found to closely follow the dashed lines. A constant shift of about 10 per cent can be seen between the dashed and coloured lines, indicating that the overall normalization may be slightly different, but the profile shapes are very similar. For old stars, the high-[α/Fe] AVR seems to flatten more strongly than for the low-[α/Fe] AVR. We note that this effect is only prominent for samples other than GALAH-MSTO, which also happen to have larger age uncertainties as compared to the GALAH-MSTO sample. Given that high-[α/Fe] stars are expected to lie in a narrow range in age, large uncertainties in age can easily flatten the AVR. Hence, large age uncertainties seem to be the most likely reason for the apparent flattening of the AVR.

Downloaded from https://academic.oup.com/mnras/article/506/2/1761/6307041 by INAF Trieste (Osservatorio Astronomico di Trieste) user on 13 April 2022

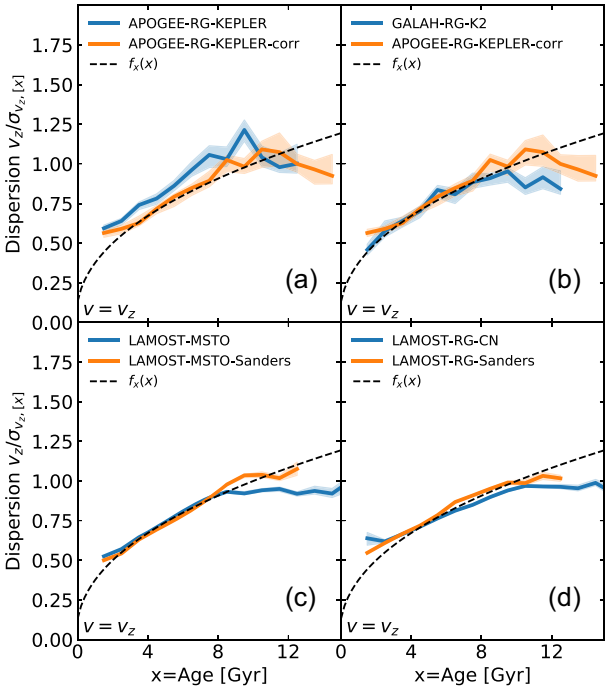

Figure 12. Velocity dispersion as a function of age for different data sets. The 16 and 84 percentile confidence interval is denoted by the shaded region. The dependences on other independent variables (L_z, [Fe/H], and $|z|$) have been divided out (see Section 3.2). The data set APOGEE-RG-KEPLER-corr was generated from APOGEE-RG-KEPLER by correcting the metallicity and age by the following transformations $[\mathrm{Fe/H}]_{\mathrm{corr}} = [\mathrm{Fe/H}] - 0.1$ and $\tau_{\mathrm{corr}} = 1.1\tau$. The velocity dispersion seems to saturate when using ages from the LAMOST value added catalogue. In comparison, no such saturation is seen when using ages from the Sanders & Das (2018) catalogue.

5.7 Testing the accuracy of the asteroseismic ages

Giants are intrinsically bright and hence for a given apparent magnitude limit they can probe a much larger Galactic volume as compared to MSTO stars. However, it is difficult to estimate the ages of giants from purely spectroscopic parameters. Over the past decades, asteroseismology has attempted to break this barrier, backed by very precise time-series photometry from space missions like CoRot, *Kepler*, and K2. However, measuring ages of a large numbers of stars often requires the use of asteroseismic scaling relations, which are empirical. Testing the accuracy of these scaling relations is complicated by the fact that it is difficult to get independent and precise measurements of mass or age of giants. A few techniques that have been used to verify the asteroseismic ages are, to assume that metal poor stars ([Fe/H]<-1) are older than 10 Gyr (Epstein et al. 2014), to use eclipsing binaries for estimating the mass (Gaulme et al. 2013; Brogaard et al. 2018), or to use cluster members to estimate the age Brogaard et al. (2012). While these studies suggest that the asteroseismic scaling relations overestimate masses by about 10 per cent, they are severely hampered by small number statistics.

An indirect means to verify asteroseismic ages is to rely on ensemble statistics – for example, by comparing the mass distribution of stars against predictions of population-synthesis-based models of the Galaxy. Sharma et al. (2016, 2017) using *Kepler* data suggested that the asteroseismic scaling-based masses were overestimated by about 10 per cent compared to model predictions. However, a follow-up study by Sharma et al. (2019) using data from both *Kepler* and K2 showed that much of the tension between observations and

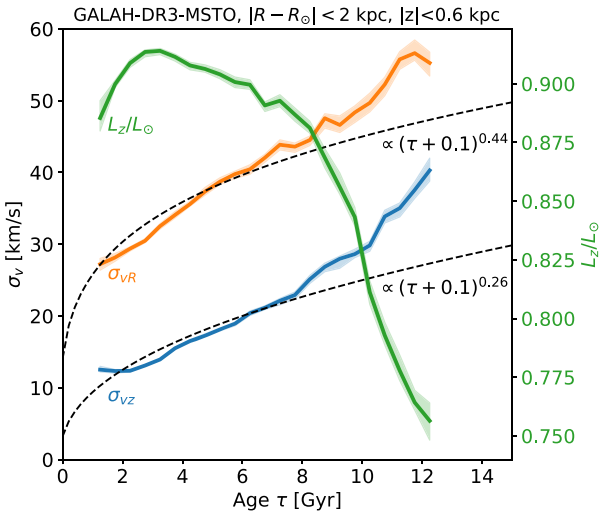

Figure 13. Velocity dispersion as a function of age for stars in the solar neighbourhood. Plotted alongside is median angular momentum as a function of age. Dashed lines show power-law profiles. For age greater than 8 Gyr, the velocity dispersion breaks away from the plotted power-law profiles, and this break coincides with a fall in angular momentum.

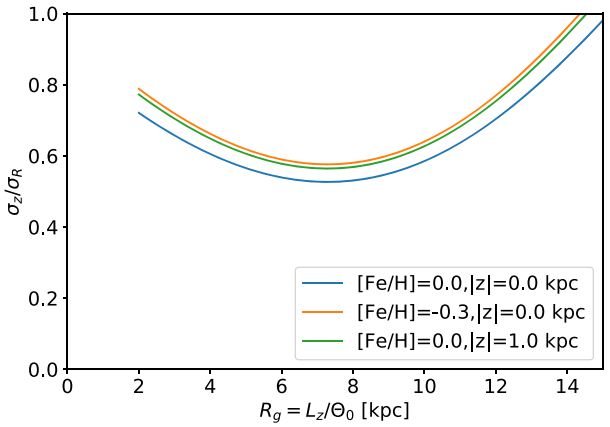

Figure 14. The ratio σ_z/σ_R as a function of guiding radius for stars of different age and metallicity. The ratio is estimated using the analytical model described by equation (3) and parameters in Table 2.

predictions is reduced after updating the metallicity of the thick disc to recent iron abundance measurements, and additionally taking α-element abundance into account. However, we still do not have a Galactic model with all its free parameters tightly constrained. In fact certain parameters are degenerate. Hence, it is useful to look for alternative methods to verify the asteroseismic ages.

Here, we provide another method to verify asteroseismic ages based on ensemble statistics – comparing the velocity dispersion of stars conditional on age, metallicity, angular momentum, and distance from the plane. The underlying principle is that the velocity dispersion is a global Galactic property. Hence, groups of stars having same age, metallicity, angular momentum, and distance from the plane should have same velocity dispersion, irrespective of their stellar type, target selection, and age estimation technique. Using the above method, we find that the conditional velocity dispersion of the GALAH-RG-K2 asteroseismic sample is in agreement with that of the GALAH-MSTO sample. The APOGEE-RG-KEPLER sample was found to have an offset with respect to the GALAH-

Downloaded from https://academic.oup.com/mnras/article/506/2/1761/6307041 by INAF Trieste (Osservatorio Astronomico di Trieste) user on 13 April 2022

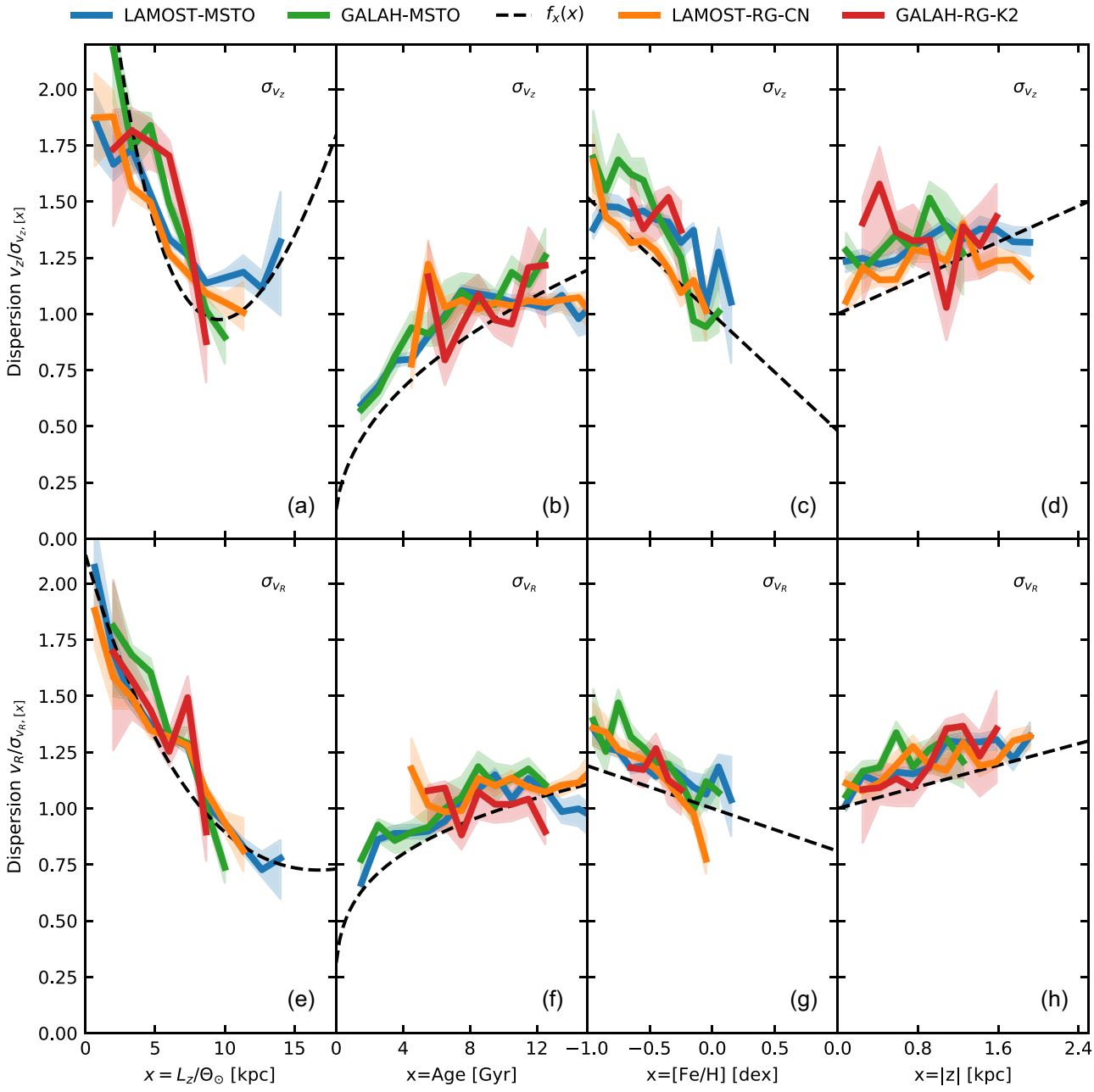

Figure 15. Same as Fig. 1 but for stars with [α/Fe]>0.25. The high-[α/Fe] stars seem to follow the same relationship as low-[α/Fe] stars, except for a small shift in the overall normalization.

MSTO sample. However, part of this offest is due to APOGEE iron abundance being higher by about 0.1 dex than GALAH. To account for the rest of the observed offset, the APOGEE-RG-KEPLER asteroseismic ages had to be increased by about 10 per cent. This bias is consistent, both in direction and amount, with earlier analysis that compared the mass distribution of the *Kepler* sample with predictions from stellar-population-synthesis based models (Sharma et al. 2019).

We now demonstrate that a 10 per cent systematic in age can easily stem from inaccuracies in measurement of average seismic parameters $\Delta\nu$ or $\nu_{\rm max}$. Pinsonneault et al. (2018) had shown that different methods for measuring $\nu_{\rm max}$ and $\Delta\nu$ can have systematics of up to a few per cent. Given that the K2 light curve is much shorter (3 months as compared to 4 yr) and is more noisy, we can also expect biases of up to a few per cent in the seismic parameters estimated from them. We show below that even a 1 per cent change in either $\Delta\nu$ or $\nu_{\rm max}$ can lead to a change of 10 per cent in age. The age of a red giant star is primarily determined by the time it spends on the main sequence and is roughly $\tau_{\rm MS} \propto M/L(M) \propto M^{-3.8}$ for stars with $M < 2{\rm M}_\odot$ (Binney & Merrifield 1998). According to asteroseismic scaling relations $M \propto \nu_{\rm max}^3/\Delta\nu^4$, implying that the age depends on $\nu_{\rm max}$ and $\Delta\nu$ with a power greater than 10.

6 SUMMARY AND CONCLUSIONS

We have explored the fundamental relations governing the radial and the vertical velocity dispersions of stars in the Milky Way and discussed the dynamical processes that might be responsible for them. For the first time, we present the joint dependence of the

Downloaded from https://academic.oup.com/mnras/article/506/2/1761/6307041 by INAF Trieste (Osservatorio Astronomico di Trieste) user on 13 April 2022

vertical and radial velocity dispersions on age, angular momentum (L_z), metallicity ([Fe/H]), and distance from the plane ($|z|$). We compare and contrast results from three different spectroscopic surveys (GALAH, LAMOST, and APOGEE) and three different stellar types (MSTO, asteroseismic giant, and RGB stars).

Vertical and radial velocity dispersions depend upon at least four independent variables, and these are age, angular momentum, metallicity, and distance from the plane. The joint dependence is well approximated by a separable functional form that is a product of univariate functions, with each function corresponding to one independent variable. In other words, the dependence of the dispersions on each independent variable is to a good extent independent of the other variables.

The velocity dispersions increase with age (for a given L_z, [Fe/H], and $|z|$) following a power law, with exponent $\beta_z = 0.441 \pm 0.007$ for σ_z and $\beta_R = 0.251 \pm 0.006$ for σ_R. These exponents are in good agreement with idealized simulations of Aumer et al. (2016b) where the disc heating is due to scattering by bar, spiral arms, and GMCs.

The velocity dispersions show a non-monotonic behaviour with L_z (for a given age, [Fe/H] and $|z|$). They decrease with L_z until about solar angular momentum, thereafter, σ_R flattens, while σ_z increases. The flattening at large L_z could be due to a non-zero floor on the intrinsic birth dispersion of stars. The rise of σ_z at large L_z could be due to a number of processes like orbiting satellites, warps, the infall of misaligned gas, and reorientation of the disc that have been associated to flaring (Minchev et al. 2015). Idealized simulations having a bar, spiral structure, and GMCs do not show such an effect. However, cosmological simulations by Minchev et al. (2014a) and Grand et al. (2016) do show a rise in σ_z at large L_z, where the effect is primarily attributed to orbiting satellites. The phase space spiral seen in *Gaia* DR2 is additional evidence of the fact that orbiting satellite (the Sagittarius dwarf in this case) can alter the kinematics of the disc stars (Bland-Hawthorn et al. 2019; Bland-Hawthorn & Tepper-García 2021). This makes orbiting satellites a strong candidate for the rise of σ_z at large L_z.

The velocity dispersions decrease almost linearly with metallicity (for a given L_z, age and $|z|$), or in other words the velocity dispersion increases with birth radius. We show that this can be explained by the conservation of vertical action in stars undergoing radial migration. However, for this to work, stars migrating outwards from the inner regions should be preferentially of low velocity dispersion – the so-called provenance bias as discussed by Vera-Ciro et al. (2014) and also reported by others (Grand et al. 2016; Daniel & Wyse 2018). Additionally, external perturbations related to flaring as discussed in the previous paragraph could also be responsible for increase of dispersion with birth radius (Minchev et al. 2014a, b).

The velocity dispersions increase almost linearly with distance from the plane (for a given L_z, age, and [Fe/H]). This effect is more prominent for younger stars. Additionally, the effect is stronger for σ_z than for σ_R. This agrees with findings of Mackereth et al. (2019), using APOGEE giants. Spiral arms are responsible for in-plane scattering, while GMCs are thought to redirect the planar motion into the vertical direction (Jenkins & Binney 1990). As suggested by Mackereth et al. (2019), the longer time scale associated with GMC heating as compared to spiral heating could be responsible for the observed non-isothermality.

A particularly useful aspect of identifying the set of independent variables that govern the velocity dispersion, is that if the dispersion is characterized in terms of these variables then it is almost independent of the target selection function. This provides a means to not only compare results from different observational data sets (e.g. to test systematics in spectroscopic stellar parameters between different surveys, or systematics between different age estimation techniques), but also to compare observational results with theoretical predictions. We take advantage of this fact to show that GALAH and LAMOST results are in agreement with each other and that results from different stellar types (MSTO and giant stars) are also in agreement with each other. The ages of giant stars have been estimated using the asteroseismic scaling relations either directly (for K2 stars) or indirectly (for LAMOST RGBs). It is difficult to verify the asteroseismic scaling relations due to a shortage of independent estimates of stellar mass or age. In this sense, we provide a new technique based on ensemble statistics to verify the accuracy of the asteroseismic ages.

The velocity dispersion of the APOGEE data set of asteroseismic giants from *Kepler* was found to be systematically different from our derived relations. We identify two possible reasons for this. First, the metallicity of APOGEE giants is systematically lower by about 0.1 dex with respect GALAH and LAMOST. Second, it is possible that the average asteroseismic parameters derived from *Kepler* data have some systematics with respect to those derived from the K2 data, given that the light curves from K2 are much shorter (3 months as compared to 4 yr) and noisier.

We find that all stars, irrespective of them being old or having high-[α/Fe], follow the same relations for velocity dispersion. In other words, no special provision is needed to accommodate the thick disc stars. The AVR of stars in the solar neighbourhood does show a break from a pure power law for stars older than 8 Gyr. However, when the angular momentum and metallicity of these stars is taken into account no such break is seen. The apparent break is due to older stars having systematically lower angular momentum.

Finally, we note that we do find some departures from the multiplicative separable form used to model the velocity dispersion. This is not unexpected, given the complex process at play that affect the kinematics of the stars. However, it is not clear as to what parametric form one should assume to accommodate these departures. Alternatively, one could adopt a non-parametric approach and derive a relation over a grid on the multidimensional space defined by L_z, age, [Fe/H] and $|z|$. This approach will have good predictive power, but would be difficult to interpret physically. In future, it will be useful to explore a model with more degrees of freedom. However, to do that we need better observational data. Presently, the multidimensional space spanned by L_z, age, [Fe/H], and $|z|$ has significant regions that are sparsely sampled by observations and this needs to be improved.

ACKNOWLEDGEMENTS

SS is funded by a Senior Fellowship (University of Sydney), an ASTRO-3D Research Fellowship and JBH's Laureate Fellowship from the Australian Research Council (ARC). JBH's research team is supported by an ARC Laureate Fellowship (FL140100278) and funds from ASTRO-3D. MJH is supported by an ASTRO-3D 4-year Research Fellowship. DS is the recipient of an ARC Future Fellowship (project number FT1400147). SB and KL acknowledge funds from the Alexander von Humboldt Foundation in the framework of the Sofja Kovalevskaja Award endowed by the Federal Ministry of Education and Research. KL acknowledges funds from the Swedish Research Council (Grant 2015-00415_3) and Marie Sklodowska Curie Actions (Cofund Project INCA 600398). JK, KC, and TZ acknowledges financial support from the Slovenian Research Agency (research core funding No. P1-0188). DMN was supported by the Allan C. and Dorothy H. Davis Fellowship. JZ acknowledges support from NASA grants 80NSSC18K0391 and NNX17AJ40G. DH acknowledges support from the Alfred P. Sloan

Downloaded from https://academic.oup.com/mnras/article/506/2/1761/6307041 by INAF Trieste (Osservatorio Astronomico di Trieste) user on 13 April 2022

Foundation and the National Aeronautics and Space Administration (80NSSC19K0108). The GALAH Survey is supported by the ARC Centre of Excellence for All Sky Astrophysics in 3 Dimensions (ASTRO 3D), through project CE170100013. This work has made use of data acquired through the Australian Astronomical Observatory under programmes GALAH, TESS-HERMES and K2-HERMES. We acknowledge the traditional owners of the land on which the AAT stands, the Gamilaraay people, and pay our respects to elders past and present.

This work has made use of data from the European Space Agency (ESA) mission *Gaia* (https://www.cosmos.esa.int/gaia), processed by the *Gaia* Data Processing and Analysis Consortium (DPAC; https://www.cosmos.esa.int/web/gaia/dpac/consortium). Funding for the DPAC has been provided by national institutions, in particular the institutions participating in the *Gaia* Multilateral Agreement.

This work has made use of data from SDSS-III. Funding for SDSS-III has been provided by the Alfred P. Sloan Foundation, the Participating Institutions, the National Science Foundation, and the U.S. Department of Energy Office of Science. The SDSS-III web site is http://www.sdss3.org/.

This work has made use of Guoshoujing Telescope (the Large Sky Area Multi-Object Fiber Spectroscopic Telescope LAMOST) which is a National Major Scientific Project built by the Chinese Academy of Sciences. Funding for the project has been provided by the National Development and Reform Commission. LAMOST is operated and managed by the National Astronomical Observatories, Chinese Academy of Sciences.

DATA AVAILABILITY

The datasets were derived from sources in the public domain: [https://docs.datacentral.org.au/galah/, https://gea.esac.esa.int/archive/, http://www.sdss3.org/, http://dr4.lamost.org/].

REFERENCES

Aumer M., Binney J. J., 2009, MNRAS, 397, 1286
Aumer M., Binney J., Schönrich R., 2016a, MNRAS, 462, 1697
Aumer M., Binney J., Schönrich R., 2016b, MNRAS, 459, 3326
Aumer M., White S. D. M., 2013, MNRAS, 428, 1055
Aumer M., White S. D. M., Naab T., Scannapieco C., 2013, MNRAS, 434, 3142
Barbanis B., Woltjer L., 1967, ApJ, 150, 461
Binney J., 2012, MNRAS, 426, 1328
Binney J., Merrifield M., 1998, Galactic Astronomy, Princeton University Press, Princeton, United States
Binney J., Tremaine S., 2008, Galactic Dynamics, 2nd edn, Princeton University Press, Princeton, United States
Bland-Hawthorn J. et al., 2019, MNRAS, 486, 1167
Bland-Hawthorn J., Krumholz M. R., Freeman K., 2010, ApJ, 713, 166
Bland-Hawthorn J., Tepper-García T., 2021, MNRAS, 504, 3168
Bournaud F., Elmegreen B. G., Martig M., 2009, ApJ, 707, L1
Brogaard K. et al., 2012, A&A, 543, A106
Brogaard K. et al., 2018, MNRAS, 476, 3729
Buder S. et al., 2018, MNRAS, 478, 4513
Buder S. et al., 2021, MNRAS
Carlberg R. G., Sellwood J. A., 1985, ApJ, 292, 79
Daniel K. J., Wyse R. F. G., 2018, MNRAS, 476, 1561
De Silva G. M. et al., 2015, MNRAS, 449, 2604
De Simone R., Wu X., Tremaine S., 2004, MNRAS, 350, 627
Deng L.-C. et al., 2012, Res. Astron. Astrophys., 12, 735
Edvardsson B. et al., 1993, A&A, 500, 391
Epstein C. R. et al., 2014, ApJ, 785, L28
Förster Schreiber N. M. et al., 2009, ApJ, 706, 1364
Frankel N., Sanders J., Rix H.-W., Ting Y.-S., Ness M., 2019, ApJ, 884, 99
Freeman K. C., 1991, in Sundelius B., ed., Dynamics of Disc Galaxies, Proceedings of the conference held 25-30 May 1991 at Varberg Castle, Sweden. p. 15
Freeman K., Bland-Hawthorn J., 2002, ARA&A, 40, 487
Gaia Collaboration, 2018, A&A, 616, A1
Gaulme P., McKeever J., Rawls M. L., Jackiewicz J., Mosser B., Guzik J. A.,2013, ApJ, 767, 82
Grand R. J. J., Springel V., Gómez F. A.,Marinacci F., Pakmor R., Campbell D. J. R., Jenkins A., 2016, MNRAS, 459, 199
Grenon M., 1972, in Cayrel de Strobel G., Delplace A. M., eds, IAU Colloq. 17: Age des Etoiles. p. 55
Hänninen J., Flynn C., 2002, MNRAS, 337, 731
Hayden M. R. et al., 2020, MNRAS, 493, 2952
Ida S., Kokubo E., Makino J., 1993, MNRAS, 263, 875
Jenkins A., Binney J., 1990, MNRAS, 245, 305
Jurić M. et al., 2008, ApJ, 673, 864
Kallinger T. et al., 2010, A&A, 522, A1
Kallinger T. et al., 2014, A&A, 570, A41
Kazantzidis S., Bullock J. S., Zentner A. R., Kravtsov A. V., Moustakas L. A., 2008, ApJ, 688, 254
Kordopatis G. et al., 2015, MNRAS, 447, 3526
Lacey C. G., 1984, MNRAS, 208, 687
Lindegren L. et al., 2018, A&A, 616, A2
Mackereth J. T. et al., 2017, MNRAS, 471, 3057
Mackereth J. T. et al., 2019, MNRAS, 489, 176
Majewski S. R. et al., 2017, AJ, 154, 94
Marigo P. et al., 2017, ApJ, 835, 77
Martig M., Minchev I., Flynn C., 2014, MNRAS, 443, 2452
Martinez-Medina L. A., Pichardo B., Pérez-Villegas A., Moreno E., 2015, ApJ, 802, 109
Minchev I. et al., 2014b, ApJ, 781, L20
Minchev I. et al., 2018, MNRAS, 481, 1645
Minchev I. et al., 2019, MNRAS, 487, 3946
Minchev I., 2016, Astron. Nachr., 337, 703
Minchev I., Chiappini C., Martig M., 2014a, A&A, 572, A92
Minchev I., Famaey B., 2010, ApJ, 722, 112
Minchev I., Famaey B., Quillen A. C. Dehnen W., Martig M., Siebert A., 2012, A&A, 548, A127
Minchev I., Martig M., Streich D. Scannapieco C., de Jong R. S., Steinmetz M., 2015, ApJ, 804, L9
Minchev I., Quillen A. C., 2006, MNRAS, 368, 623
Nordström B. et al., 2004, A&A, 418, 989
Pinsonneault M. H. et al., 2018, ApJS, 239, 32
Piskunov N., Valenti J. A., 2017, A&A, 597, A16
Quillen A. C., Garnett D. R., 2001, in Funes J. G., Corsini E. M., eds, ASP Conf. Ser.Vol. 230, Galaxy Disks and Disk Galaxies. Astron. Soc. Pac., San Francisco, p. 87
Reid M. J., 1993, ARA&A, 31, 345
Reid M. J., Brunthaler A., 2004, ApJ, 616, 872
Robin A. C., Reylé C., Derrière S., Picaud S., 2003, A&A, 409, 523
Roškar R. et al., 2010, MNRAS, 408, 783
Roškar R., Debattista V. P., Quinn T. R., Stinson G. S., Wadsley J., 2008, ApJ, 684, L79
Saha K., Tseng Y.-H., Taam R. E., 2010, ApJ, 721, 1878
Sanders J. L., Binney J., 2015, MNRAS, 449, 3479
Sanders J. L., Das P., 2018, MNRAS, 481, 4093
Schönrich R., Binney J., 2009, MNRAS, 396, 203
Sellwood J. A., 2008, in Funes J. G., Corsini E. M., eds, ASP Conf. Ser.Vol. 396, Formation and Evolution of Galaxy Disks. Astron. Soc. Pac., San Francisco, p. 341
Sellwood J. A., 2013, ApJ, 769, L24
Sellwood J. A., Binney J. J., 2002, MNRAS, 336, 785
Sellwood J. A., Carlberg R. G., 1984, ApJ, 282, 61
Sharma S. et al., 2014, ApJ, 793, 51
Sharma S. et al., 2018, MNRAS, 473, 2004
Sharma S. et al., 2019, MNRAS, 490, 5335
Sharma S., Steinmetz M., Bland-Hawthorn J., 2012, ApJ, 750, 107

Downloaded from https://academic.oup.com/mnras/article/506/2/1761/6307041 by INAF Trieste (Osservatorio Astronomico di Trieste) user on 13 April 2022

Sharma S., Stello D., Bland-Hawthorn J., Huber D., Bedding T. R., 2016, ApJ, 822, 15
Sharma S., Stello D., Huber D., Bland-Hawthorn J., Bedding T. R., 2017, ApJ, 835, 163
Shiidsuka K., Ida S., 1999, MNRAS, 307, 737
Silva Aguirre V. et al., 2018, MNRAS, 475, 5487
Solway M., Sellwood J. A., Schönrich R., 2012, MNRAS, 422, 1363
Spitzer Lyman J., Schwarzschild M., 1951, ApJ, 114, 385
Stello D. et al., 2015, ApJ, 809, L3
Ting Y.-S., Rix H.-W., 2019, ApJ, 878, 21
Valenti J. A., Piskunov N., 1996, A&AS, 118, 595
van der Kruit P. C., 1988, A&A, 192, 117
Velazquez H., White S. D. M., 1999, MNRAS, 304, 254
Vera-Ciro C., D'Onghia E., Navarro J., Abadi M., 2014, ApJ, 794, 173
Villalobos A., Helmi A., 2008, MNRAS, 391, 1806
Wisnioski E. et al., 2015, ApJ, 799, 209
Wu Y. et al., 2019, MNRAS, 484, 5315
Xiang M. et al., 2017a, ApJS, 232, 2
Xiang M. S. et al., 2017b, MNRAS, 467, 1890
Zhao G., Zhao Y.-H., Chu Y.-Q., Jing Y.-P., Deng L.-C., 2012, Res. Astron. Astrophys., 12, 723

[1]*Sydney Institute for Astronomy, School of Physics, The University of Sydney, NSW 2006, Australia*
[2]*ARC Centre of Excellence for All Sky Astrophysics in Three Dimensions (ASTRO-3D), ACT 2611, Australia*
[3]*School of Physics, University of New South Wales, Sydney, NSW 2052, Australia*
[4]*Stellar Astrophysics Centre, Department of Physics and Astronomy, Aarhus University, DK-8000 Aarhus C, Denmark*
[5]*Max Planck Institute for Astronomy (MPIA), Koenigstuhl 17, D-69117 Heidelberg, Germany*
[6]*Research School of Astronomy & Astrophysics, Australian National University, ACT 2611, Australia*
[7]*Institute of Astrophysics, University of Vienna, Türkenschanzstrasse 17, Vienna 1180, Austria*
[8]*Max Planck Institute for Astrophysics, Karl-Schwarzschild-Str. 1, D-85741 Garching, Germany*
[9]*Department of Physics & Astronomy, Macquarie University, Sydney, NSW 2109, Australia*
[10]*INAF -Osservatorio Astronomico di Padova, Padova 35122, Italy*
[11]*Faculty of Mathematics and Physics, University of Ljubljana, Jadranska 19, 1000 Ljubljana, Slovenia*
[12]*Department of Astronomy, Stockholm University, AlbaNova University Center, SE-106 91 Stockholm, Sweden*
[13]*Centre for Astrophysics, University of Southern Queensland, Toowoomba, Queensland 4350, Australia*
[14]*Research Centre in Astronomy, Astrophysics & Astrophotonics, Macquarie University, Sydney, NSW 2109, Australia*
[15]*Institute for Astronomy, University of Hawai'i, 2680 Woodlawn Drive, Honolulu, HI 96822, USA*
[16]*International Centre for Radio Astronomy Research (ICRAR), The University of Western Australia, 35 Stirling Highway, Crawley, WA 6009, Australia*
[17]*Institute for Advanced Study, Princeton, NJ 08540, USA*
[18]*Department of Astrophysical Sciences, Princeton University, Princeton, NJ 08544, USA*
[19]*Observatories of the Carnegie Institution of Washington, 813 Santa Barbara Street, Pasadena, CA 91101, USA*
[20]*Department of Physics and Astronomy, The Johns Hopkins University, Baltimore, MD 21218, USA*
[21]*Department of Fiqh and Usul, Academy of Islamic Studies, University of Malaya, 50603 Kuala Lumpur, Malaysia*
[22]*Sydney Institute for Astronomy, School of Physics, A28, The University of Sydney, NSW 2006, Australia*
[23]*Exoplanetary Science at UNSW, School of Physics, University of New South Wales, Sydney, NSW 2052, Australia*
[24]*Lund Observatory, Department of Astronomy and Theoretical Physics, Box 43, SE-221 00 Lund, Sweden*
[25]*Department of Industry, Innovation and Science, 105 Delhi Rd, North Ryde, NSW 2113, Australia*

This paper has been typeset from a TEX/LATEX file prepared by the author.

Downloaded from https://academic.oup.com/mnras/article/506/2/1761/6307041 by INAF Trieste (Osservatorio Astronomico di Trieste) user on 13 April 2022